

Pump-Probe Faraday Rotation and Ellipticity in an Ensemble of Singly Charged Quantum Dots

I. A. Yugova

Institute of Physics, St. Petersburg State University, 198504 St.-Petersburg, Russia

M. M. Glazov and E. L. Ivchenko

Ioffe Physical-Technical Institute RAS, 194021 St.-Petersburg, Russia

Al. L. Efros

Naval Research Laboratory, Washington DC 20375, USA

(Dated: October 31, 2018)

A description of spin Faraday rotation, Kerr rotation and ellipticity signals for single- and multi-layer ensembles of singly charged quantum dots (QDs) is developed. The microscopic theory considers both the single pump-pulse excitation and the effect of a train of such pulses, which in the case of long resident-electron spin coherence time leads to a stationary distribution of the electron spin polarization. The calculations performed for single-color and two-color pump-probe setups show that the three experimental techniques: Faraday rotation, Kerr rotation and ellipticity measurements provide complementary information about an inhomogeneous ensemble of QDs. The microscopic theory developed for a three-dimensional ensemble of QDs is shown to agree with the phenomenological description of these effects. The typical time-dependent traces of pump-probe Faraday rotation, Kerr rotation and ellipticity signals are calculated for various experimental conditions.

PACS numbers: 78.67.Hc, 78.47.-p, 71.35.-y

I. INTRODUCTION

It is impossible to overestimate the role, which pump-probe spin Faraday and Kerr rotation measurements have played and continue to play in developing of spintronics, a new area of science and technology that tries to utilize an electron spin, in addition to its charge, in various semiconductor devices^{1,2}. The discovery of a very long spin coherence time in bulk GaAs³ and II-VI compound quantum wells⁴ using these highly sensitive techniques was one of the cornerstones for the initiation of spintronics, and today pump-probe spin-dependent spectroscopy has become a common way to study carrier spin coherence in bulk crystals^{5,6}, quantum wells (QWs)^{7,8} and quantum dot (QD) samples^{9,10,11,12,13}. At the same time Kerr rotation measurements have become the most visual and impressive method to study electron spin transport^{14,15}, spin accumulation and injection^{16,17}, and the spin-Hall effect^{18,19}.

The schematic illustration of the pump-probe measurement techniques is shown in Fig. 1. A first short intense pulse of circularly polarized light (a pump pulse) generates the nonequilibrium spin-oriented electrons and holes and creates a macroscopic spin polarization²⁰. In a constant transverse magnetic field, \mathbf{B} , applied to the sample the macroscopic polarization starts to precess around the field direction. On the microscopic single-spin level, the precession is connected with a coherent superposition of two spin levels split by the magnetic field. The superposition is created by a short pulse of circularly polarized light and the quantum mechanical beating of this coherent superposition occurs at the Larmor precession frequency of the applied magnetic field, $\Omega_L = g_e \mu_B B / \hbar$,

where g_e is the electron g -factor, and μ_B is the Bohr magneton. The optically created polarization and its precession can be probed by short pulses of linearly polarized light via rotation of their polarization plane after the propagation through the photoexcited medium (Faraday effect) or reflection from this medium (Kerr effect). The short probe pulses of linearly polarized light show a remarkable sensitivity to the practically instant population of electron and hole spin sublevels. The pump-probe techniques allow one to study spin dynamics of resident carriers that are also polarized by the pump pulse during their coherence time, which exceeds the typical photoluminescence decay time by several orders of magnitude. These advantages make the pump-probe Faraday and Kerr rotation techniques suggested more than 15 years ago^{21,22,23,24} to be a powerful tool to study the carrier spin dynamics.

The pump-probe spin-dependent rotation techniques are especially useful for manipulation and measurement on electron spin polarization in singly charged QDs due to a very long coherence time of resident-electron spins. This time in QDs could be as long as several microseconds^{11,25} and it exceeds the spin coherence time measured in bulk GaAs^{3,26} by two orders of magnitude. The resonant short pulse excitation of such QDs by circularly polarized light leads to practically deterministic creation of an electron spin polarization¹³. A train of such pump pulses results in complete synchronization of electron spins if their precession frequency satisfies the phase synchronization condition (PSC), which is fulfilled when the train repetition period being shorter than the single electron spin coherence time is equal to an integer number of the Larmor precession periods²⁷. This syn-

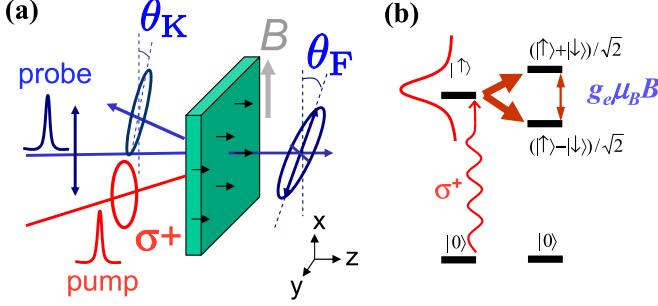


FIG. 1: Schematic illustration of (a) the pump-probe Faraday and Kerr rotation measurement techniques and (b) a coherent superposition created by a short pulse of σ^+ polarized light from the two spin states split in a transverse magnetic field, B . θ_F and θ_K are the Faraday and Kerr rotation angles, respectively.

chronization leads to the mode locking of electron spin coherence in an ensemble of QDs¹¹, the effect which allows one to overcome the dephasing of electron spin polarization connected with a dispersion of precession frequencies and to control the ensemble polarization during a single electron spin coherence time. The mode-locking effect in self-organized (In,Ga)As/GaAs QDs is enhanced by the nuclear induced frequency focusing effect, which shifts the electron spin precession frequencies of the entire ensemble of QDs to the modes satisfying the PSC²⁸. This last phenomenon opens exciting opportunities to create an entire ensemble of QDs with more than one million spins having a single precession frequency²⁹ and their controlled manipulation by short pulses of various polarizations^{30,31}.

Despite the tremendous success of the pump-probe Faraday and Kerr rotation measurement techniques, their microscopic theoretical descriptions for QD structures are absent to the best of our knowledge. For bulk semiconductors and QWs the theory of magneto-optical photoinduced Faraday effect was developed, respectively, by Aronov and Ivchenko³² and by the authors of Refs.^{7,33,34}. In the present paper we develop such a theory for the array of QDs considered as an ensemble of independent localized oscillating dipoles. This approximation, which generally imposes a restriction on the QD concentration, is usually sufficiently accurate in self-organized QD samples like those used, e.g., in Ref.¹³.

In the standard pump-probe Faraday rotation experiments, the transmitted probe light is split into two linearly polarized beams with orthogonal polarizations oriented at $\pm 45^\circ$ angles relative to the initial light polarization (or the polarization of the probe light transmitted through the unpumped sample). Then the difference of the time-integrated intensities of the split beams is measured as a function of the delay between pump and probe pulses³⁵. To describe the experimental setup we introduce two pairs of axes, x, y and x', y' , rotated by

a 45° angle with respect to each other. The initial polarization of the probe light is along x axis. This allows us to define the experimentally measured spin Faraday signal, \mathcal{F} , as

$$\mathcal{F} = \lim_{z \rightarrow +\infty} \int_0^{T_{\text{exp}}} \left[|E_{x'}^{(t)}(z, t)|^2 - |E_{y'}^{(t)}(z, t)|^2 \right] dt, \quad (1)$$

where $E_{x'}^{(t)}(z, t)$ and $E_{y'}^{(t)}(z, t)$ are respectively the x' - and y' -components of an electric field of the transmitted probe light at time t . They are connected with the x - and y -components of the electric field: $E_{x'} = (E_x - E_y)/\sqrt{2}$ and $E_{y'} = (E_x + E_y)/\sqrt{2}$. Equation (1) assumes the probe light source to be positioned at $z \rightarrow -\infty$.

In this form Eq. (1) is derived for the case where the sample is subject to a periodic train of pump and probe pulses repeated with a certain period T_R . The integration in Eq. (1) takes place over the measurement time, T_{exp} , which exceeds by far all other time constants in the experiment, such as spin precession and relaxation times and pulse repetition period. For the case of a single pump and single probe pulse the integration in Eq. (1) is effectively carried out during the probe pulse duration, τ_p .

The Kerr effect is measured in the reflection geometry and its magnitude is defined as

$$\mathcal{K} = \lim_{z \rightarrow -\infty} \int_0^{T_{\text{exp}}} \left[|E_{x'}^{(r)}(z, t)|^2 - |E_{y'}^{(r)}(z, t)|^2 \right] dt, \quad (2)$$

where $E_{x'}^{(r)}(z, t)$ and $E_{y'}^{(r)}(z, t)$ are respectively the x' - and y' -components of the reflected probe pulse electric field. The probe-pulse rotation angles in the Faraday and Kerr rotation measurements can approximately be expressed in a simple form³⁶

$$\theta_F \approx \mathcal{F}/2\mathcal{I}, \quad \theta_K \approx \mathcal{K}/2\mathcal{I}, \quad (3)$$

if $|\theta_{F,K}| \ll 1$. Here \mathcal{I} is the total time-integrated intensity of the transmitted or reflected probe pulse, respectively.

The pump-probe ellipticity measurement is another way to study spin dynamics in samples photoexcited by the polarized pump pulse³⁷. The experimental setup in this case is similar to setup used for the Faraday rotation measurements but with $1/4$ waveplate. The ellipticity signal in transmission is defined by the following integrated difference

$$\mathcal{E} = \lim_{z \rightarrow +\infty} \int_0^{T_{\text{exp}}} \left[|E_{\sigma^-}^{(t)}(z, t)|^2 - |E_{\sigma^+}^{(t)}(z, t)|^2 \right] dt, \quad (4)$$

where $E_{\sigma^\pm}^{(t)} = (E_x^{(t)} \mp iE_y^{(t)})/\sqrt{2}$ are the circular σ^+ and σ^- components of the transmitted probe pulse. For small ellipticity values, the so-called angle of ellipticity, ε , is given by

$$\varepsilon \approx \mathcal{E}/2\mathcal{I}. \quad (5)$$

In this paper we calculate microscopically the magnitudes of the single- and two-color pump-probe Faraday and Kerr rotation signals, \mathcal{F} and \mathcal{K} , and the ellipticity signal \mathcal{E} in an ensemble of singly charged QDs resonantly excited by a single short light pulse of an arbitrary shape or an infinite train of such pulses. The calculations show that the three measurement techniques explore spin polarization properties of different subsets of QDs due to inhomogeneous broadening of the resonant transition energies in the QD ensemble, and the results of these measurements may be nonidentical. As a result, the time-dependent traces measured by these three techniques significantly differ from each other and are very sensitive functions of the pump and probe excitation frequencies, their detuning, and the dependence of the electron g -factor and the oscillator transition strength on the trion excitation frequencies. The traces of the Kerr rotation signal depend also on the thickness of the cap layer. The average electron spin precession frequencies measured in these experiments can differ as well.

Our paper is organized as follows. In Sec. II we provide a theoretical description of electron spin polarization created in an ensemble of QDs by a single short pulse of circularly polarized light or by an infinite train of such pulses. The general microscopic theory of probing this spin polarization in the QD ensemble is presented in Sec. III. For a three-dimensional ensemble of QDs we compare the developed approach with the standard phenomenological description of magneto-optical pump-probe effects within the effective-medium approximation. In the final Sec. IV we calculate typical time-dependent traces of the two color pump-probe Faraday and Kerr rotation and the ellipticity signals and briefly compare the obtained results with available experimental data.

II. CREATION OF ELECTRON SPIN POLARIZATION IN SINGLY CHARGED QUANTUM DOTS

In what follows we consider a planar array of singly charged zinc blende based QDs grown along the axis $z \parallel [001]$. The QDs are self-organized during molecular beam epitaxy growth on the wetting layer. The lateral size remarkably exceeds their height, which serves a quantization axis for the electron $\pm 1/2$ spin states and heavy-hole $\pm 3/2$ spin states responsible for the dominating optical transitions. In the absence of a magnetic field, the ground state of a singly charged QD is two-fold spin degenerate. The first excited state of such a QD under interband transitions is a singlet trion, which consists of two electrons occupying the same size-quantized level with opposite spins and a heavy hole in one of the two degenerate states: $\pm 3/2$. The optical selection rules for the resonant excitation of these trion states and their radiative decay are very restrictive. The $+3/2$ trion states can be created only by the σ^+ circularly polarized light and only in a QD where the resident electron has the

spin projection $+1/2$. These $+3/2$ trion states can radiatively decay only into the initial $+1/2$ spin states. At the same time σ^+ circularly polarized light does not affect an electron with the spin projection $-1/2$. The same rules with the sign reversal “+” \leftrightarrow “-” are applied for the optical excitation of the $-3/2$ trion state. It is important to notice that the singlet trion in these QDs does not have an optical transition dipole component along the z axis.

A. Pumping of electron spins in quantum dots

Let us first consider the effect of QD photoexcitation by a short electromagnetic pulse with the carrier frequency ω_p close to the trion resonant frequency ω_0 . We also assume that the pulse duration time τ_p is short compared with other times: the spin relaxation times of a resident electron and a photohole forming the trion; the trion radiative lifetime; and the spin precession period of an electron and a heavy hole in an external magnetic field. According to the selection rules the interaction of the QD with the electromagnetic wave is described by the Hamiltonian

$$\hat{V}(t) = - \int [\hat{d}_+(\mathbf{r})E_{\sigma^+}(\mathbf{r}, t) + \hat{d}_-(\mathbf{r})E_{\sigma^-}(\mathbf{r}, t)]d^3r, \quad (6)$$

where $\hat{d}_{\pm}(\mathbf{r}) = [\hat{d}_x(\mathbf{r}) \pm i\hat{d}_y(\mathbf{r})]/\sqrt{2}$ are the circularly polarized components of the dipole moment density operator, and $E_{\sigma_{\pm}}(\mathbf{r}, t)$ are the circularly polarized components of the electric field of a quasi monochromatic electromagnetic wave. The electric field of this wave is defined as

$$\mathbf{E}(\mathbf{r}, t) = E_{\sigma^+}(\mathbf{r}, t)\mathbf{o}_+ + E_{\sigma^-}(\mathbf{r}, t)\mathbf{o}_- + \text{c.c.}, \quad (7)$$

where \mathbf{o}_{\pm} are the circularly polarized unit vectors related to the unit vectors $\mathbf{o}_x \parallel x$ and $\mathbf{o}_y \parallel y$ by $\mathbf{o}_{\pm} = (\mathbf{o}_x \pm i\mathbf{o}_y)/\sqrt{2}$. Here the both components E_{σ^+} and E_{σ^-} are proportional to the exponential function $e^{-i\omega_p t}$.

The incident electromagnetic field induces optical transitions between the electron state and the trion state creating a coherent superposition of them. In accordance with the selection rules the σ^+ circularly polarized light creates a superposition of the $+1/2$ electron and $+3/2$ trion states while the σ^- polarized light creates a superposition of the $-1/2$ electron and $-3/2$ trion states. In order to describe these superpositions it is convenient to introduce a four component wavefunction

$$\Psi = (\psi_{1/2}, \psi_{-1/2}, \psi_{3/2}, \psi_{-3/2}), \quad (8)$$

where the $\pm 1/2$ subscripts denote the electron spin projection and $\pm 3/2$ refer to the spin projection of a hole in the trion. The electron spin polarization is expressed in terms of $\psi_{\pm 1/2}$ as follows

$$\begin{aligned} S_z &= (|\psi_{1/2}|^2 - |\psi_{-1/2}|^2) / 2, \\ S_x &= \text{Re}(\psi_{1/2}\psi_{-1/2}^*), \quad S_y = -\text{Im}(\psi_{1/2}\psi_{-1/2}^*). \end{aligned} \quad (9)$$

Hereafter we completely neglect all other excited states of a QD, e.g., triplet trion states, and treat the QD optical excitation within the four-level model. In this approximation the action of a short pulse on the charged QD can be described by the following equations

$$i\hbar\dot{\psi}_{3/2} = \hbar\omega_0\psi_{3/2} + V_+(t)\psi_{1/2}, \quad (10)$$

$$i\hbar\dot{\psi}_{1/2} = V_+^*(t)\psi_{3/2},$$

$$i\hbar\dot{\psi}_{-3/2} = \hbar\omega_0\psi_{-3/2} + V_-(t)\psi_{-1/2}, \quad (11)$$

$$i\hbar\dot{\psi}_{-1/2} = V_-^*(t)\psi_{-3/2}.$$

Here $\dot{\psi} \equiv \partial\psi/\partial t$ and the time-dependent matrix elements $V_{\pm}(t) = -\int d(\mathbf{r})E_{\sigma_{\pm}}(\mathbf{r}, t)d^3r$ describe the light interaction with a QD. The strength of this interaction is characterized by the effective transition dipole³⁸

$$\begin{aligned} \mathbf{d}(\mathbf{r}) &= \langle 1/2|\hat{d}_-(\mathbf{r})|3/2\rangle = \langle -1/2|\hat{d}_+(\mathbf{r})|-3/2\rangle \\ &= -i\frac{ep_{cv}}{\omega_0 m_0}\mathbf{F}(\mathbf{r}, \mathbf{r}), \end{aligned} \quad (12)$$

which is the matrix element of the operators $\hat{d}_{\pm}(\mathbf{r})$ in Eq. (6) calculated between the wave functions of the valence band, $|\pm 3/2\rangle$, and the conduction band, $|\pm 1/2\rangle$, all taken in the electron representation. In Eq. (12), e is the electron charge, m_0 is the free electron mass, and $p_{cv} = \langle \mathbf{S}|\hat{p}_x|\mathbf{X}\rangle = \langle \mathbf{S}|\hat{p}_y|\mathbf{Y}\rangle = \langle \mathbf{S}|\hat{p}_z|\mathbf{Z}\rangle$ is the interband matrix element of the momentum operator taken between the conduction- and valence-band Bloch functions at the Γ point of the Brillouin zone, \mathbf{S} and $(\mathbf{X}, \mathbf{Y}, \mathbf{Z})$, respectively. Finally,³⁹

$$\mathbf{F}(\mathbf{r}_e, \mathbf{r}_h) = \varphi_h(\mathbf{r}_h)\varphi_e^{(\text{tr})}(\mathbf{r}_e) \int d^3r'\varphi_e(\mathbf{r}')\varphi_e^{(\text{tr})}(\mathbf{r}'), \quad (13)$$

where $\varphi_e^{(\text{tr})}$ and φ_h are, respectively, the electron and heavy-hole envelope functions in a trion, and φ_e is the envelope function of a single (resident) electron confined in a QD. These wave functions are chosen to be real. In derivation of Eq. (13) we assumed that the QD is small enough so that the electron and hole motion in a trion can be treated independently, but allowed for the different orbital functions of the resident electron and the electrons in a singlet trion.⁴⁰ Note, that in Eq. (13) $\mathbf{F}(\mathbf{r}_e, \mathbf{r}_h)$ is taken at the coinciding coordinates of the carriers, $\mathbf{r}_e = \mathbf{r}_h = \mathbf{r}$.

Due to a very short timescale of the pump pulse we completely neglect the electron and hole spin precession during pulse action as well as spin dephasing and radiative decay processes in Eqs. (10) and (11). The dynamics of the electron spin polarization described by these equations was considered before in Ref.¹³ in the case of a rectangular shape pulse with the resonant carrying frequency $\omega_p = \omega_0$. This paper generalizes the consideration for detuned pulses of an arbitrary shape.

To be specific we consider the excitation of the QD by a σ^+ polarized light pulse; the difference in the dynamics of the electron spin polarization created under the

σ^- photoexcitation is briefly discussed below. Before the pump pulse arrival the QD is always in the ground state because the pump repetition period is much longer than the trion lifetime in the QD. For the σ^+ polarized excitation the component $\psi_{-1/2}$ of the QD wavefunction is conserved, and $\psi_{-3/2} \equiv 0$. This allows one to reduce the set of Eqs. (10) to a single equation for the component $\psi_{1/2}(t)$

$$\ddot{\psi}_{1/2} - \left(i\omega' + \frac{\dot{f}(t)}{f(t)} \right) \dot{\psi}_{1/2} + f^2(t)\psi_{1/2} = 0. \quad (14)$$

Here $\omega' = \omega_p - \omega_0$ is the detuning between the pump frequency and the trion resonance frequency, and $f(t)$ is a smooth envelope of pump pulse defined as

$$f(t) = -\frac{e^{i\omega_p t}}{\hbar} \int d(\mathbf{r})E_{\sigma^+}(\mathbf{r}, t)d^3r.$$

It follows from Eq. (14) that the values $\psi_{1/2}$ and $\dot{\psi}_{1/2}$ before and after the pulse action are connected linearly⁴¹. Taking into account that the initial conditions for Eqs. (10) are $\psi_{1/2}(-\infty) = \text{const}$, $\psi_{3/2}(-\infty) = 0$ and, therefore, $\dot{\psi}_{1/2}(-\infty) = 0$, one can represent the solution of Eq. (14) at $t \gg \tau_p$, i.e., after the pulse is over, as

$$\psi_{1/2}(\infty) = Qe^{i\Phi}\psi_{1/2}(-\infty). \quad (15)$$

Here the real coefficient Q satisfies the condition $0 \leq Q \leq 1$ and the phase Φ can be chosen in the interval between $-\pi$ and π . Both parameters are determined by the pump pulse shape, power and detuning. Equations (9) and (15) determine the modification of the electron spin polarization from a short pulse of an arbitrary shape. Taking into account that $\psi_{-1/2}$ is conserved under the σ^+ polarized excitation, the electron spin before the pulse arrival, $\mathbf{S}^- = (S_x^-, S_y^-, S_z^-)$, and just after the end of the pulse, $\mathbf{S}^+ = (S_x^+, S_y^+, S_z^+)$, are connected by

$$S_z^+ = \frac{Q^2 - 1}{4} + \frac{Q^2 + 1}{2}S_z^-, \quad (16a)$$

$$S_x^+ = Q \cos \Phi S_x^- + Q \sin \Phi S_y^-, \quad (16b)$$

$$S_y^+ = Q \cos \Phi S_y^- - Q \sin \Phi S_x^-. \quad (16c)$$

Although Eqs. (16) are derived for the pure spin states they are valid as well for the mixed states whenever the pulse duration τ_p is much shorter than the spin relaxation times in the QD and the time of electron and hole spin precession in a transverse magnetic field.

Using Eqs. (10) one can show that $|\psi_{1/2}(t)|^2 + |\psi_{3/2}(t)|^2 = |\psi_{1/2}(-\infty)|^2$. It follows then that the z component of the post-pulse trion spin polarization formally defined as $J_z = (|\psi_{3/2}(\infty)|^2 - |\psi_{-3/2}(\infty)|^2)/2$ is equal to

$$J_z = S_z^- - S_z^+. \quad (17)$$

Derivation of the relation between \mathbf{S}^+ and \mathbf{S}^- established by the σ^- circularly-polarized pulse gives equations similar to Eqs. (16). One has, however, to change the sign of the first term in Eq. (16a) and replace Φ by $-\Phi$ in Eqs. (16b) and (16c).

Equations (16) and (17) are the main result of this Section. They show how the short pulses of circularly polarized light create and control the electron spin polarization in n -type QDs under the resonant trion excitation. At low pump intensities the electron spin is weakly affected and a value of $Qe^{i\Phi}$ slightly deviates from unity. For high intensities the coefficient Q noticeably decreases and the phase Φ shifts from zero. One can see from Eq. (16a) that the σ^+ circularly polarized pulse modifies the z -component of electron spin polarization by $S_z^+ - S_z^- = (Q^2 - 1)(1 + 2S_z^-)/4$. The pump pulse also leads to the in-plane rotation of the electron spin polarization along the light propagation direction for pulses with $\Phi \neq 0$ (see Eqs. (16b) and (16c)) similarly to spin rotation in a longitudinal magnetic field $\mathbf{B} \parallel z$.

It is easy to show that the phase Φ becomes nonzero due to detuning between the resonant and pump frequencies. Indeed, under resonant conditions, $\omega' = 0$, or small detuning, $\omega'\tau_p \ll 1$, one can neglect $i\omega'$ as compared with $\dot{f}(t)/f(t) \sim \tau_p^{-1}$ in Eq. (14) and produce the solution in the form

$$\psi_{1/2}(t) = \psi_{1/2}(-\infty) \cos \left[\int_{-\infty}^t f(t') dt' \right]. \quad (18)$$

The direct comparison with Eq. (15) gives $\Phi \equiv 0$ and $Q = \cos(\Theta/2)$, where

$$\Theta = 2 \int_{-\infty}^{\infty} f(t') dt' \quad (19)$$

is the effective pulse area. This consideration shows that only detuned pump pulses give rise to $\Phi \neq 0$ and generate an effective magnetic field acting on an electron spin in the QD. The pulse tuned resonantly to the trion transition causes no rotation of the in-plane spin components, and the electron spin dynamics is independent of the pulse shape and is controlled only by the pulse area Θ .

Let us now analyze the dependence of Q and Φ on the pulse parameters for the detuned pulses. In the general case of an arbitrary pump pulse power, its arbitrary detuning and shape, Eq. (14) can be solved only numerically. The analytical solutions of Eq. (14) are known for the two pulse shapes: (i) for pulses with rectangular shape, $f(t) = f_0 \equiv \text{const} \neq 0$ for $|t| < \tau_p/2$ and $f(t) = 0$ otherwise, (ii) for smooth pulses of the shape suggested by Rosen and Zener⁴²:

$$f(t) = \frac{\mu}{\cosh(\pi t/\tau_p)}, \quad (20)$$

where the coefficient μ is a measure of the pulse electric field strength. The effective areas of these pulses are equal to $\Theta = 2f_0\tau_p$ and $\Theta = 2\mu\tau_p$, respectively.

For $f(t)$ taken in the form of Eq. (20) one can write the solution of Eq. (14) following Ref.⁴² in terms of the hypergeometric function

$$\psi_{1/2}(t) = \psi_{1/2}(-\infty) \times {}_2F_1 \left[\frac{\Theta}{2\pi}, -\frac{\Theta}{2\pi}; \frac{1}{2} - iy; \frac{1}{2} \tanh\left(\frac{\pi t}{\tau_p}\right) + \frac{1}{2} \right], \quad (21)$$

where $\Theta = 2\mu\tau_p$ and the dimensionless detuning $y = \omega'\tau_p/(2\pi)$. This leads to explicit expressions for Q and Φ :

$$Q = \left| \frac{\Gamma^2(\frac{1}{2} - iy)}{\Gamma(\frac{1}{2} - \frac{\Theta}{2\pi} - iy) \Gamma(\frac{1}{2} + \frac{\Theta}{2\pi} - iy)} \right| = \sqrt{1 - \frac{\sin^2(\Theta/2)}{\cosh^2(\pi y)}}, \quad (22)$$

$$\Phi = \arg \left\{ \frac{\Gamma^2(\frac{1}{2} - iy)}{\Gamma(\frac{1}{2} - \frac{\Theta}{2\pi} - iy) \Gamma(\frac{1}{2} + \frac{\Theta}{2\pi} - iy)} \right\}. \quad (23)$$

In the case of a rectangular shaped pulse we obtain

$$Q = \sqrt{1 - \frac{\Theta^2}{x^2} \sin^2 \frac{x}{2}}, \quad (24)$$

$$\Phi = \pi y - \phi, \quad (25)$$

where $\Theta = 2f_0\tau_p$, effective Rabi frequency

$$x = \sqrt{(2\pi y)^2 + \Theta^2}, \quad (26)$$

and $\sin \phi = (y/Qx) \sin(x/2)$. One can see from Eqs. (23) and (25) that Φ changes its sign with reversal of the detuning parameter y . For circularly polarized pump pulses, this means that the sign of detuning determines the rotation direction of the electron spin polarization and its reversal is similar to switching the effective magnetic field from one direction to the opposite.

According to Eqs. (16) and (17) the reorientation of electron spin polarization by short pulses with $Q = 0$ or $Q = 1$ becomes deterministic and can be used for controllable manipulation of a single electron spin. The pump pulses with $Q = 0$ completely erase, for any detuning, the in-plane spin components^{13,31} leading to the alignment of the electron spin along the z axis. On the other hand, the pulses with $Q = 1$ lead to a controllable rotation of the electron spin in the (x, y) plane and make no effect on the spin z component. The rotation angle equals to Φ and is determined by the detuning³¹. It follows from Eqs. (22)–(25) that the value $Q = 0$ can be reached only with the pulses tuned to the resonance ($y = 0$) and having the areas $\Theta = \pi, 3\pi, \dots$ (the so-called π -pulses). In the case of Rosen&Zener pulses³¹ the condition $Q = 1$ is realized for any detuning if $\Theta = 2\pi, 4\pi, \dots$ (2π -pulses). For the rectangular pulses this condition can be reached only for certain combinations of the detuning and pulse area when the effective Rabi frequency $x = \sqrt{(2\pi y)^2 + \Theta^2} = 2\pi N$ with N being an integer.

Figure 2 shows the calculated dependences of Q and Φ on the detuning for four pulse areas Θ , each for rectangular and Rosen&Zener pulse shapes. For large detuning, $y = |\omega_p - \omega_0|\tau_p/2\pi \gg 1$, Q is close to 1, Φ tends to 0. Therefore, the electron spin state in a QD is unaffected by the strongly detuned pulses. For the area $\Theta = \pi$, the function $Q(y)$ has a sharp dip at $y = 0$ reaching zero value at this particular point. Thus, for π -pulses tuned to the resonance ω_0 the parameter Q vanishes and, as stated above, the pump pulses suppress the transverse spin components S_x^+ and S_y^+ . Deviation of Θ from π converts the dip into a smooth minimum. In accordance

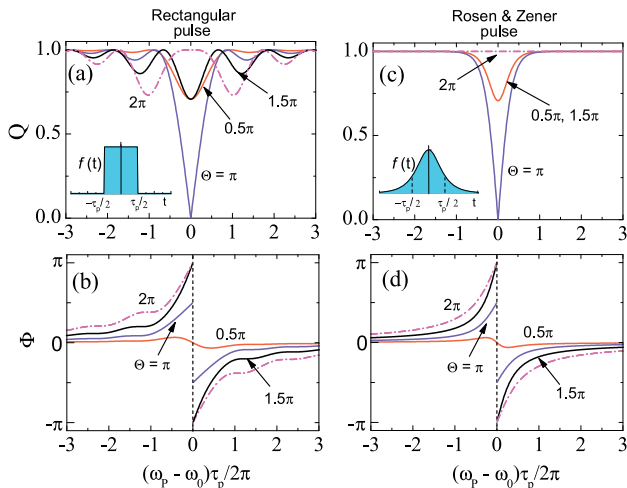


FIG. 2: Dependence of Q and Φ on detuning $y = (\omega_p - \omega_0)\tau_p/2\pi$ for pulses having the rectangular shape (a,b) and Rosen&Zener shape (c,d) calculated for several pulse areas $\Theta = \pi/2, \pi, 3\pi/2, 2\pi$. Insets demonstrate shapes of pulses.

with Eq. (22), the pulses with the areas Θ and $2\pi - \Theta$ produce the same Q . The signs of the phase Φ and detuning are opposite, and Φ makes, at zero detuning, an abrupt jump from its positive maximum value to the negative minimum value. The altitude of this jump rises along with the pump pulse area. Although the both pulse shapes lead to generally similar dependences of Q or Φ on the detuning, the rectangular shape pulses give rise to additional oscillations on the curves $Q(y), \Phi(y)$ clearly seen in Figs. 2(a), 2(b). These oscillations are connected with the oscillating character of the Fourier transform of a rectangular shaped signal. They are absent for the Rosen-Zener pulse, for the general case of a smooth pulse these oscillations are much weaker than for the rectangular pulse. One can see that, for $\Theta \neq \pi$, $Q(y)$ has several minima at $y \neq 0$. This occurs because at these detuning the effective Rabi frequency, x , approaches to the $N\pi$ with $N = 1, 3, 5, \dots$

Figure 3 compares the z -component S_z^+ of electron spin polarization created by rectangular (dash-dot black curves) and Rosen&Zener (solid red curves) pulses of different areas Θ in singly charged QDs with zero spin,

$S_z^- = 0$, before the pulse arrival. One can see that the rectangular pulses with $\Theta > \pi$ result in intensive oscillations of S_z^+ at large-scale detuning, whereas oscillations are completely absent for the Rosen&Zener pulses. The oscillations are again connected with the shape of the Fourier transform of a rectangular signal. One can see in Fig. 3(d) that detuned pulses of a different shape create a completely different electron spin polarization.

B. Temporal dynamics of electron and trion spin polarization after the pulse

The temporal dynamics of electron and trion spin polarization in a QD after its excitation by the short pump pulse can be determined from the kinetic equations for the electron spin polarization \mathbf{S} and z -component J_z of the trion spin polarization^{7,13,27}

$$\begin{aligned} \dot{\mathbf{S}} + \mathbf{S} \times \boldsymbol{\Omega} + \frac{\mathbf{S}}{\tau_{s,e}} &= \frac{J_z \mathbf{o}_z}{\tau_{QD}}, \\ \dot{J}_z + \frac{J_z}{\tau_{QD}} + \frac{J_z}{\tau_{s,h}} &= 0. \end{aligned} \quad (27)$$

The equations take into account (i) the precession of electron spins in the in-plane magnetic field \mathbf{B} with frequency $\boldsymbol{\Omega}$, (ii) the electron spin relaxation, (iii) the spin relaxation of a hole in the trion, (iv) the radiative decay of the trion, and, finally, (v) the partial suppression of the electron spin polarization created by the pulse after the trion recombination. It is ignoring, however, the hole precession. Here $\tau_{s,e}$, $\tau_{s,h}$ and τ_{QD} are the single electron spin relaxation time, the hole spin relaxation time and the trion lifetime, respectively.

The detailed analysis of the spin dynamics in the coupled electron-trion system has been carried out in Refs.^{7,27} (see also^{43,44}). It is instructive to consider the simplest case of these dynamics when the hole-in-trion spin relaxation is much faster than the trion radiative lifetime, $\tau_{s,h} \ll \tau_{QD}$, or when the electron spin precession time $2\pi/\Omega \ll \tau_{QD}$. In the both limits the electron remaining in the QD after the trion recombination becomes completely depolarized and its contribution to the electron spin polarization created during the pulse is completely negligible^{11,13}. In this case the precession of electron spin polarization in a transverse magnetic field after the trion decay is described by the following set of equations¹¹

$$\begin{aligned} S_z(t) &= [S_z^+ \cos \Omega t + S_y^+ \sin \Omega t] e^{-t/\tau_{s,e}}, \\ S_y(t) &= [S_y^+ \cos \Omega t - S_z^+ \sin \Omega t] e^{-t/\tau_{s,e}}, \\ S_x(t) &= S_x^+ e^{-t/\tau_{s,e}}, \end{aligned} \quad (28)$$

where time t is referred to the end of excitation pulse, and the electron spin polarization components S_α^+ ($\alpha = x, y, z$) created by the pulse are defined by Eqs. (16).

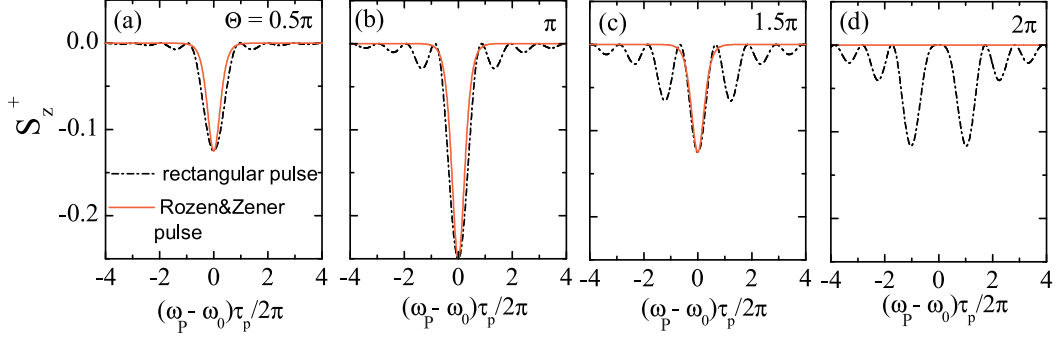


FIG. 3: Effect of detuning $\omega_p - \omega_0$ on the z -component of electron spin polarization, S_z^+ , created by the rectangular (dash-dot black curves) and Rosen&Zener (solid red curves) pulses. Curves are calculated using Eq. (16a) with $S_z^- = 0$ and Eqs. (22, 24) for the pulse areas: $\Theta = 0.5\pi$ (a), π (b), 1.5π (c), and 2π (d).

C. Electron spin polarization created in QDs by an infinite train of short pulses

In the pump-probe Faraday and Kerr rotation experiments the sample is usually subjected to a train of pump pulses that follow with a certain repetition period T_R . If the time T_R is comparable with or smaller than the single electron spin relaxation time in a QD, $T_R \leq \tau_{s,e}$, the electrons retain the memory of being exposed to the previous pulses. The infinite train of pulses creates a steady state of the electron spin polarization in the QDs periodically varying in time with the same period T_R , which leads to a number of remarkable phenomena such as the resonant spin amplification^{3,43} and the mode locking of electron spin coherence^{11,12}. The time evolution between the pulses is described by Eq. (28) where S_α^+ ($\alpha = x, y, z$) are the components of spin polarization taken at the end of any pump pulse. To find these components one should associate the polarization (28) at the moment $t = T_R$ with the spin polarization at the moment before arrival of the next pulse, $\mathbf{S}(T_R) \equiv \mathbf{S}^-$, and interconnect it with \mathbf{S}^+ according to Eqs. (16). As a result we obtain self-consistent equations for the components S_α^+ . Solving them and substituting the solution into Eqs. (16) we find the components S_α^- which can be written as

$$\begin{aligned}
 S_x^- &= K S_y^-, \\
 S_y^- &= \frac{1 - Q^2}{4\Delta} e^{-\frac{T_R}{\tau_{s,e}}} \sin(\Omega T_R), \\
 S_z^- &= \frac{1 - Q^2}{4\Delta} e^{-\frac{T_R}{\tau_{s,e}}} \times \\
 &\quad \left[Q(\cos \Phi - K \sin \Phi) e^{-\frac{T_R}{\tau_{s,e}}} - \cos(\Omega T_R) \right], \tag{29}
 \end{aligned}$$

where

$$\begin{aligned}
 \Delta &= 1 - e^{-T_R/\tau_{s,e}} \times \\
 &\quad \left[\frac{1 + Q^2}{2} + Q(\cos \Phi - K \sin \Phi) \right] \cos(\Omega T_R) \\
 &\quad + \frac{Q(1 + Q^2)}{2} e^{-2T_R/\tau_{s,e}} (\cos \Phi - K \sin \Phi), \\
 K &= \frac{Q e^{-T_R/\tau_{s,e}} \sin \Phi}{1 - Q e^{-T_R/\tau_{s,e}} \cos \Phi}. \tag{30}
 \end{aligned}$$

One can check that, for a periodic train of pulses of arbitrary intensity and shape, the electron spin polarization reaches the highest value at the magnetic field satisfying the PSC condition $\Omega = 2\pi N/T_R$, where N is an integer^{3,11,12,43}. For such electrons $\cos(\Omega T_R) = 1$ and the z -component of their spin polarization at the moment of pulse arrival can be written as

$$S_z^- = -\frac{1}{2} \frac{1 - Q^2}{2e^{T_R/\tau_{s,e}} - 1 - Q^2}. \tag{31}$$

Equation (31) shows that the maximum value of $|S_z^-|$ is independent of the phase shift Φ between $\psi_{1/2}(\infty)$ and $\psi_{1/2}(-\infty)$. For pulses with $Q = 1$ the orientation of electron spins does not occur since such pulses rotate the in-plane spin components but do not generate the spin coherence. Quite often the pulse repetition period used in experiments is much shorter than spin relaxation time: $T_R \ll \tau_{s,e}$ ¹³. This allows to rewrite Eq. (31) as

$$S_z^- \approx -\frac{1}{2} \frac{1}{1 + 2T_R/[\tau_{s,e}(1 - Q^2)]}. \tag{32}$$

One can see that even in the case of weak excitation where $1 - Q^2 \ll 1$ the electron spin satisfying the PSC reaches its utmost alignment $S_z^- \approx -1/2$ if

$$2 \frac{T_R}{\tau_{s,e}} \ll 1 - Q^2 = \frac{\sin^2(\Theta/2)}{\cosh^2(\pi y)}. \tag{33}$$

The latter equality is valid for Rosen&Zener pulses. For the large ratio $\tau_{s,e}/T_R$ even quite detuned pulses, e.g.,

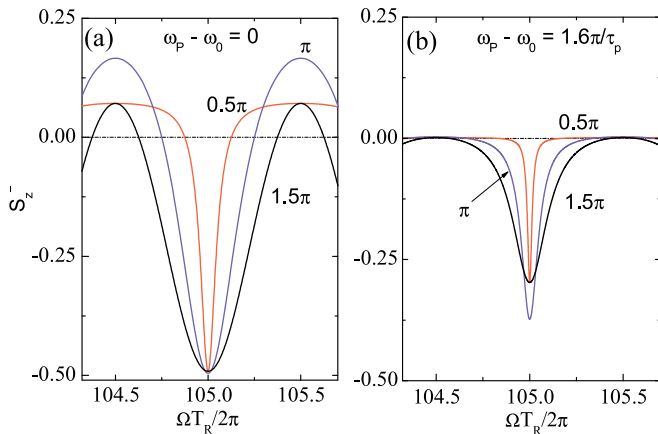


FIG. 4: Electron spin polarization, S_z^- , created by a train of Rozen&Zener pump pulses with the repetition frequency $T_R = 13.2$ ns at the moment of pulse arrival as a function of the electron spin precession frequency Ω . Dependences shown on panels (a) and (b) are calculated, respectively, for zero detuning between the pump frequency and quantum dot frequency, $\omega_p = \omega_0$, and for the detuning $\omega_p - \omega_0 = 1.6\pi/\tau_p$. The chosen pulse areas are $\Theta = 0.5\pi, \pi$ and 1.5π . For g -factor from Ref.¹¹ the value of $\Omega T_R/2\pi = 105$ is reached at a magnetic field $B = 1$ T. The calculations used $\tau_{s,e} = 3$ μ s from Ref.¹¹.

with $(\omega_p - \omega_0)\tau_p \sim 3$, are still quite efficient in the spin alignment. A train of weak pulses, however, synchronizes electron spin precession only in a very narrow frequency range around the PSC. As a result the frequency dependence of $S_z^-(\Omega)$ created by such a train has a periodic form with sharp minima at the frequencies satisfying the PSC

$$S_z^- \propto \left[(\Omega T_R - 2\pi N)^2 + \frac{T_R^2}{\tau_{s,e}^2} + \Phi^2 + (1-Q)^2 + 2\frac{T_R}{\tau_{s,e}}(1-Q) \right]^{-1}. \quad (34)$$

Here it is assumed that $1-Q \ll 1$, $T_R \ll \tau_{s,e}$ and $\Phi \ll 1$. The width of the minima is proportional to

$$\frac{1}{T_R} \sqrt{\left(\frac{T_R}{\tau_{s,e}}\right)^2 + 2(1-Q)\frac{T_R}{\tau_{s,e}} + (1-Q)^2 + \Phi^2},$$

i.e., it is determined either by the spin relaxation rate $\tau_{s,e}^{-1}$ or by the effective pump area $1-Q$ and phase Φ . Figure 4 shows just one period of this dependence.

The modulation of the electron spin polarization $S_z^-(\Omega)$ becomes weaker with the increasing detuning. For example, assuming $\Phi = \pm\pi/2$ and using the condition $T_R \ll \tau_{s,e}$ one can derive for arbitrary Q

$$S_z^-(\Omega) = -\frac{1}{2} \frac{Q^2 + \cos \Omega T_R}{Q^2 + 2 - \cos \Omega T_R}, \quad (35)$$

which is a much smoother function of Ω .

For the π -pulse excitation ($Q \rightarrow 0$) which can be realized only in the absence of detuning ($\Phi = 0$) we arrive at¹¹

$$S_z^- = -\frac{1}{2} \frac{\cos \Omega T_R}{2 - \cos \Omega T_R}. \quad (36)$$

The polarization S_z^- reaches its minimum value $-1/2$ when the electron spin precession frequency satisfies the PSC condition.

For a given pulse shape the phase Φ and the factor Q are interconnected and, in general, a change of the pulse area results in changes of both Q and Φ . Figure 4 shows the z component of electron spin polarization, S_z^- , at the moment of pulse arrival calculated as a function of the Larmor frequency for different pulse areas under resonant excitation and for nonzero detuning. One can see from Fig. 4(a) that for zero detuning ($\Phi = 0$) and small pulse areas, S_z^- exhibits a sharp minimum as a function of Larmor precession frequency in agreement with the above analytical considerations. The increase of the pulse area transforms this minimum to the cosine-like curve.

Figure 4(b) shows $S_z^-(\Omega)$ created by an appreciably detuned pulse train, $\omega_p - \omega_0 = 1.6\pi/\tau_p$. In agreement with Fig. 2 the effective pump power in this case is small, i.e., Q is close to 1. An increase of the pump area from $\pi/2$ to π leads to a small decrease of Q and a nonzero value of Φ . As a result the minimum at the spin precession frequency Ω satisfying the PSC becomes deeper and wider. The further increase of the pump area results in additional widening of the minimum due to the increase of Φ but its depth becomes smaller since Q starts to increase.

III. PROBING SPIN DYNAMICS IN QUANTUM DOTS

The detection of the QD spin polarization in pump-probe Faraday and Kerr rotation experiments is carried out by a linearly polarized probe pulse. The electric field of the probe pulse shown in Fig. 1 oscillates along the x axis and similarly to Eq. (7) it can be written as

$$E^{\text{pr}}(\mathbf{r}, t) = E_x^{\text{pr}}(\mathbf{r}, t) \frac{\mathbf{o}_+ + \mathbf{o}_-}{\sqrt{2}} + \text{c.c.} \quad (37)$$

Here we assume that $E_x^{\text{pr}}(\mathbf{r}, t) \propto e^{-i\omega_{\text{pr}}t}$, where ω_{pr} is the carrying frequency of the probe light. In order to calculate Faraday and Kerr rotation angles of polarization plane of the probe pulse as well as the ellipticity we first find the QD polarization induced by the probe field and then calculate the secondary electric field induced by the QD array.

A. Probe-induced polarization of QDs

Before the probe pulse arrival the electronic state of a QD is described by the wavefunction (8). We consider

the general case where the QD is characterized by the population of the electron $n_e = |\psi_{1/2}|^2 + |\psi_{-1/2}|^2$ and trion $n_t = |\psi_{3/2}|^2 + |\psi_{-3/2}|^2$ states and the spin polarization of these states $S_z = (|\psi_{1/2}|^2 - |\psi_{-1/2}|^2)/2 \neq 0$ and $J_z = (|\psi_{3/2}|^2 - |\psi_{-3/2}|^2)/2 \neq 0$, respectively. Solving Eqs. (10), (11) in the lowest order in \mathbf{E}^{pr} we find the probe-induced corrections to the electron and trion components of the wave function

$$\begin{aligned}\delta\psi_{\pm 3/2} &= \psi_{\pm 1/2} \int_{-\infty}^t \frac{V(t')}{i\hbar} e^{-i\omega_0(t-t')} dt', \\ \delta\psi_{\pm 1/2} &= \psi_{\pm 3/2} \int_{-\infty}^t \frac{V^*(t')}{i\hbar} e^{i\omega_0(t-t')} dt',\end{aligned}\quad (38)$$

where

$$V(t) = -\frac{1}{\sqrt{2}} \int d(\mathbf{r}) E_x^{\text{pr}}(\mathbf{r}, t) d^3r. \quad (39)$$

The electron-trion superposition excited in a QD by the light pulses creates a local polarization, whose magnitude depends on the components of the wave function

described in Eq. (8). According to the selection rules, the circular components of the QD dielectric polarization can be written as

$$\begin{aligned}P_{\sigma+}(\mathbf{r}) &= \mathbf{d}^*(\mathbf{r})(\psi_{3/2} + \delta\psi_{3/2})(\psi_{1/2} + \delta\psi_{1/2})^* + \text{c.c.}, \\ P_{\sigma-}(\mathbf{r}) &= \mathbf{d}^*(\mathbf{r})(\psi_{-3/2} + \delta\psi_{-3/2})(\psi_{-1/2} + \delta\psi_{-1/2})^* \\ &\quad + \text{c.c.},\end{aligned}\quad (40)$$

where the effective transition dipole is defined by Eq. (12). In Eqs. (40) the zero-order contributions, which are proportional to $\psi_{3/2}\psi_{1/2}^*$ and $\psi_{-3/2}\psi_{-1/2}^*$, determine the QD emission due to the presence of photoexcited trions. They make no contribution to the measured pump-probe rotation signal and will not be considered further. The other contributions in Eqs. (40) are induced by the probe pulse. The Faraday and Kerr rotation of the probe light polarization as well as its ellipticity are determined only by the terms linear in $\delta\psi_{\pm 1/2}$ and $\delta\psi_{\pm 3/2}$. Combining Eqs. (40) we can write the linearly polarized components of the QD polarization induced by the probe pulse as follows

$$\begin{aligned}\delta P_x^{QD}(\mathbf{r}, t) &= -\frac{n_e - n_{tr}}{2i\hbar} \mathbf{d}^*(\mathbf{r}) \int d^3r' \int_{-\infty}^t dt' e^{i\omega_0(t'-t)} d(\mathbf{r}') E_x^{\text{pr}}(\mathbf{r}', t') + \text{c.c.}, \\ \delta P_y^{QD}(\mathbf{r}, t) &= -\frac{S_z - J_z}{\hbar} \mathbf{d}^*(\mathbf{r}) \int d^3r' \int_{-\infty}^t dt' e^{i\omega_0(t'-t)} d(\mathbf{r}') E_x^{\text{pr}}(\mathbf{r}', t') + \text{c.c.}\end{aligned}\quad (41)$$

The light wavelength is usually much larger than the size of self-organized QDs. This allows one to extract the probe electric field $E_x^{\text{pr}}(\mathbf{r}', t')$ from the integral and present the QD polarization in the approximate δ -function-like form

$$\delta P_\alpha^{QD}(\mathbf{r}, \mathbf{R}_j, t) = \delta(\mathbf{r} - \mathbf{R}_j) \Pi_\alpha(\mathbf{R}_j, t) \quad (\alpha = x, y),$$

where \mathbf{R}_j is the position of j -th QD. The resulting probe-field induced polarization of a single QD can be expressed as

$$\Pi_x(\mathbf{R}_j, t) = -\frac{n_e - n_{tr}}{2i\hbar} |\mathcal{D}|^2 \int_{-\infty}^t e^{i\omega_0(t'-t)} E_x^{\text{pr}}(\mathbf{R}_j, t') dt' + \text{c.c.}, \quad (42)$$

$$\Pi_y(\mathbf{R}_j, t) = -\frac{S_z - J_z}{\hbar} |\mathcal{D}|^2 \int_{-\infty}^t e^{i\omega_0(t'-t)} E_x^{\text{pr}}(\mathbf{R}_j, t') dt' + \text{c.c.}, \quad (43)$$

via the integral QD transition dipole $\mathcal{D} = \int d^3r d(\mathbf{r})$ related to the two-particle wave function $F(\mathbf{r}, \mathbf{r})$:

$$|\mathcal{D}|^2 = \frac{e^2 |p_{cv}|^2}{\omega_0^2 m_0^2} \left| \int F(\mathbf{r}, \mathbf{r}) d^3r \right|^2.$$

As one can see from Eqs. (41) the probe-induced QD polarization δP^{QD} consists of two components. The first, δP_x^{QD} , is parallel to the probe polarization plane and its magnitude is proportional to the difference of

electron and trion occupation numbers. The second component, δP_y^{QD} , is orthogonal to the probe polarization plane and its magnitude is proportional to the difference of the electron and trion spin polarizations. The latter

polarization component is responsible for the probe-pulse polarization plane rotation, i.e., spin Faraday and Kerr effects, and for circular dichroism (ellipticity of the transmitted or reflected probe beam). Note that the appearance of the δP_y^{QD} component is not a direct consequence of the spin-orbit interaction: this component is not relativistically small as compared with δP_x^{QD} .

B. Circular birefringence and dichroism induced by photoexcited QDs

Once the probe-induced dielectric polarization of the QD is known, it is possible to calculate an electric field induced by the QD ensemble and, therefore, find the probe polarization plane rotation and ellipticity. First we consider an experimental situation where pumping and probing are carried out on a planar array of QDs. Then we generalize the results to a stack of such QD planes and a bulk array of QDs.

Let us consider a layer of self-organized QDs forming the plane $z = 0$. The total electric field \mathbf{E} ⁴⁵ in the system can be represented as a sum of the incident electric field $\mathbf{E}_0^{\text{pr}}(t)e^{iqz}$ and the electric field induced by the QD dielectric polarization $\delta\mathbf{P}^{QD}$. The field \mathbf{E} satisfies the electromagnetic wave equations

$$\Delta\mathbf{E}(\mathbf{r}, t) - \text{grad div } \mathbf{E}(\mathbf{r}, t) = -\left(\frac{\omega_{\text{pr}}}{c}\right)^2 \mathbf{D}, \quad (44)$$

$$\text{div } \mathbf{D} = 0, \quad (45)$$

with the material equation

$$\mathbf{D}(\mathbf{r}, t) = \varepsilon_b \mathbf{E}(\mathbf{r}, t) + 4\pi \mathbf{P}_{\text{tot}}(\mathbf{r}, t). \quad (46)$$

Here ε_b is the dielectric constant of the cap layer assumed to coincide with the background dielectric constant of the QDs; $\mathbf{P}_{\text{tot}}(\mathbf{r}, t) = \sum_j \delta\mathbf{P}^{QD}(\mathbf{r}, \mathbf{R}_j, t)$ is the sum of the probe-induced polarizations over all QDs; \mathbf{D} is the displacement field; ω_{pr} is the carrying frequency; and c is the speed of light in vacuum. Although the pumping and probing of QDs is performed by short pulses, their duration τ_p is assumed to exceed by far the period of electro-magnetic field oscillations $2\pi/\omega_{\text{pr}}$. Therefore, the solutions of Eqs. (44)-(46) are quasi-monochromatic waves with slowly varying amplitudes.

It follows from Eq. (45) that $\text{div } \mathbf{E} = -(4\pi/\varepsilon_b) \text{div } \mathbf{P}_{\text{tot}}(\mathbf{r})$ which allows us to rewrite Eq. (44) in the form

$$\Delta\mathbf{E}(\mathbf{r}, t) + q^2 \mathbf{E}(\mathbf{r}, t) = -4\pi \left(\frac{\omega_{\text{pr}}}{c}\right)^2 (1 + q^{-2} \text{grad div}) \mathbf{P}_{\text{tot}}(\mathbf{r}, t), \quad (47)$$

where $q = \omega_{\text{pr}}\sqrt{\varepsilon_b}/c$. By introducing the Green's function for the three-dimensional space

$$G(\mathbf{r}) = \frac{\exp(iqr)}{4\pi r}, \quad (48)$$

Eq. (47) can further be transformed into an integral equation

$$\mathbf{E}(\mathbf{r}, t) = \mathbf{E}_0^{\text{pr}}(t)e^{iqz} + 4\pi \left(\frac{\omega_{\text{pr}}}{c}\right)^2 \int d^3r' G(\mathbf{r} - \mathbf{r}') (1 + q^{-2} \text{grad div}) \mathbf{P}_{\text{tot}}(\mathbf{r}', t). \quad (49)$$

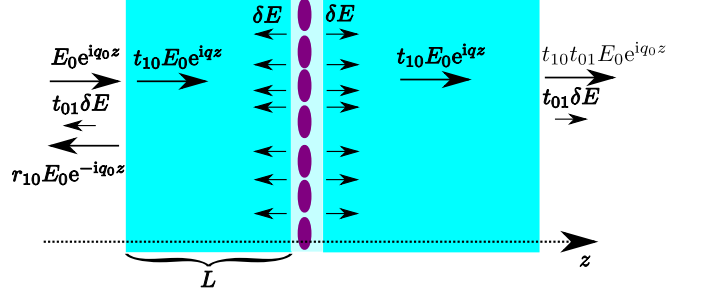


FIG. 5: Schematic image of the light propagation in a QD structure, which contains a QD layer overgrown by a cap layer of the thickness L . Long arrows show the transmission and reflection of the incident probe light (with the electric-field amplitude E_0) on the external surface while short arrows illustrate the creation of the secondary field, δE , due to scattering of the transmitted light by QDs. r_{10} , t_{10} and t_{01} are the corresponding reflection and transmission coefficients.

A plane wave of the probe electromagnetic field propagating along the z direction creates a dielectric polarization in QDs randomly distributed in the plane $z = 0$. Assuming the interdot distances to be smaller than the light wavelength one can neglect the $q^{-2} \text{grad div}$ term in the integral of Eq. (49) and average $\mathbf{P}_{\text{tot}}(\mathbf{r})$ over the distribution of QDs. As a result we can replace $\mathbf{\Pi}(\mathbf{R}_j, t)$ by the coordinate independent vector $\mathbf{\Pi}(t)$. This allows us to rewrite Eq. (49) in the following form

$$\mathbf{E}(\mathbf{r}, t) = \mathbf{E}_0^{\text{pr}}(t)e^{iqz} - 4\pi \left(\frac{\omega_{\text{pr}}}{c}\right)^2 \mathbf{\Pi}(t) \sum_j \int d^2\rho' dz' G(\mathbf{r} - \mathbf{r}') \delta(\rho_j - \rho') \delta(z'), \quad (50)$$

where ρ_j are the QD positions in the two-dimensional layer. Assuming that QDs in the array are identical and randomly distributed we replace the sum in Eq. (50) by the integral and arrive at

$$\mathbf{E}(\mathbf{r}, t) = \mathbf{E}_0^{\text{pr}}(t)e^{iqz} - 4\pi \left(\frac{\omega_{\text{pr}}}{c}\right)^2 \frac{i}{2q} e^{iq|z|} N_{QD}^{2D} \mathbf{\Pi}(t), \quad (51)$$

where N_{QD}^{2D} is the two-dimensional density of QDs. Deriving Eq. (51) we used the following property of two-dimensional integral

$$\int 2\pi\rho d\rho \frac{\exp(iq\sqrt{z^2 + \rho^2})}{4\pi\sqrt{z^2 + \rho^2}} = \frac{i}{2q} \exp(iq|z|),$$

which can be proven by adding a small positive imaginary part to q and setting it to $+0$.

It is convenient to represent the electric field in a QD sample as

$$\mathbf{E}(\mathbf{r}, t) = \mathbf{E}_0^{\text{pr}}(t)e^{iqz} + \delta\mathbf{E}(t)e^{iq|z|}, \quad (52)$$

where the first term is just the incident probe field and the second term describes the secondary field induced by QDs:

$$\delta\mathbf{E}(t) = -4\pi \left(\frac{\omega_{\text{pr}}}{c}\right)^2 \frac{i}{2q} N_{\text{QD}}^{2D} \mathbf{\Pi}(t). \quad (53)$$

This equation allows one to find magnitudes of the Faraday rotation signals and ellipticity.

If the sample contains M layers of QDs and the stack thickness d is smaller than the light wavelength then the second term in Eq. (52) should merely be multiplied by M . In a more conventional description of three-dimensional (3D) ensemble of QDs, the factor MN_{QD}^{2D} can be rewritten as N_{QD}^{3D} , where N_{QD}^{3D} is the 3D concentration of QDs.

The straightforward calculation shows that the Faraday rotation signal defined by Eq. (1) can be presented as

$$\mathcal{F} = -2 \int_{-\infty}^{\infty} \text{Re} [E_{0,x}^{\text{pr}*}(t) \delta E_y(t)] dt, \quad (54)$$

where only a contribution linear in $\delta\mathbf{E}$ is taken into account. Substituting δE_y from Eqs. (43) and (53) we arrive at

$$\mathcal{F} = \frac{3\pi}{q^2 \tau_{\text{QD}}} N_{\text{QD}}^{2D} (S_z - J_z) \text{Im} \left\{ \int_{-\infty}^{\infty} dt \int_{-\infty}^t dt' e^{i\omega_0(t'-t)} E_{0,x}^{\text{pr}*}(t) E_{0,x}^{\text{pr}}(t') \right\}, \quad (55)$$

where τ_{QD} is the radiative lifetime of an electron-hole pair confined in a QD:

$$\frac{1}{\tau_{\text{QD}}} = \frac{4}{3} \frac{q^3}{\varepsilon_b \hbar} |\mathcal{D}|^2. \quad (56)$$

Similarly, the calculation of the ellipticity defined by Eq. (4) results in

$$\mathcal{E} = -2 \int_{-\infty}^{\infty} \text{Im} [E_{0,x}^{\text{pr}*}(t) \delta E_y(t)] dt. \quad (57)$$

Substituting δE_y from Eqs. (43) and (53) we obtain

$$\mathcal{E} = \frac{3\pi}{q^2 \tau_{\text{QD}}} N_{\text{QD}}^{2D} (S_z - J_z) \text{Re} \left\{ \int_{-\infty}^{\infty} dt \int_{-\infty}^t dt' e^{i\omega_0(t'-t)} E_{0,x}^{\text{pr}*}(t) E_{0,x}^{\text{pr}}(t') \right\}. \quad (58)$$

In samples with a cap layer, see Fig. 5, the Faraday rotation and ellipticity signals acquire an extra factor $t_{10}t_{01}$ in Eq. (55), where t_{01} and t_{10} are the transmission coefficients through the interface from the cap layer to vacuum and vice versa, respectively.

The cap layer strongly influences the Kerr effect, i.e., the polarization plane rotation in the reflection geometry. This happens because its magnitude is determined by the interference between the probe beam reflected from the cap layer and the secondary wave induced by the QDs, see Fig. 5. The phase difference of the reflected and secondary waves is determined by the cap layer thickness L leading to the following expression for the Kerr rotation magnitude

$$\mathcal{K} = r_{01}t_{01}t_{10}[\cos(2qL)\mathcal{F} + \sin(2qL)\mathcal{E}], \quad (59)$$

where \mathcal{F} and \mathcal{E} are given by Eqs. (55) and (58), re-

spectively, and r_{01} is the reflection coefficient from the vacuum – cap layer interface. It is seen that the Kerr effect measures, in general, a superposition of the Faraday rotation and ellipticity signals.

Equations (55) and (58) demonstrate that Faraday, ellipticity, and therefore Kerr signals (see Eq.(59)) are proportional to the difference of electron and trion spin polarization in QDs: $S_z - J_z$. The magnitudes of the effects are proportional to the QD density and increase with a decrease of the radiative lifetime τ_{QD} due to an increase of the transition dipole moment.

In order to analyze the dependence of the Faraday and ellipticity signals on the detuning between probe frequency, ω_{pr} , and trion resonance frequency, ω_0 , we represent probe field as $E_0^{\text{pr}}(t) = E^{(0)}s(t)e^{-i\omega_{\text{pr}}t}$, where $s(t)$ is the envelope function. It can be seen from

Eqs. (55) and (58) that

$$\mathcal{F} \propto \text{Im} G(\omega_{\text{pr}} - \omega_0), \quad \mathcal{E} \propto \text{Re} G(\omega_{\text{pr}} - \omega_0), \quad (60)$$

where

$$G(\Lambda) = \int_{-\infty}^{\infty} dt \int_{-\infty}^t dt' s(t) s(t') e^{i\Lambda(t-t')}, \quad (61)$$

with $\Lambda = \omega_{\text{pr}} - \omega_0$. It can be recast as a half axis Fourier transform of the probe autocorrelation function

$$G(\Lambda) = \int_0^{+\infty} dt e^{i\Lambda t} \int_{-\infty}^{\infty} dt' s(t') s(t+t')$$

and calculated for particular pulse shapes as follows

$$G(\Lambda) = \begin{cases} \frac{1}{\Lambda^2} (i\Lambda\tau_p + 1 - e^{i\Lambda\tau_p}) & \text{for } s(t) = 1 \text{ if } -\tau_p/2 \leq t \leq \tau_p/2 \text{ and } s(t) = 0 \text{ otherwise,} \\ \frac{\tau_p}{\pi^2} \zeta\left(2, \frac{1}{2} - \frac{i\Lambda\tau_p}{2\pi}\right) & \text{for } s(t) = \cosh^{-1}(\pi t/\tau_p), \\ \frac{\tau_p^2}{(1 + \Lambda^2\tau_p^2)^2} (2 + i\Lambda\tau_p(3 + \Lambda^2\tau_p^2)) & \text{for } s(t) = e^{-|t|/\tau_p}, \end{cases} \quad (62)$$

where $\zeta(a, b)$ is the generalized Riemann ζ -function defined as $\zeta(a, b) = \sum_{k=0}^{\infty} (k+b)^{-a}$.

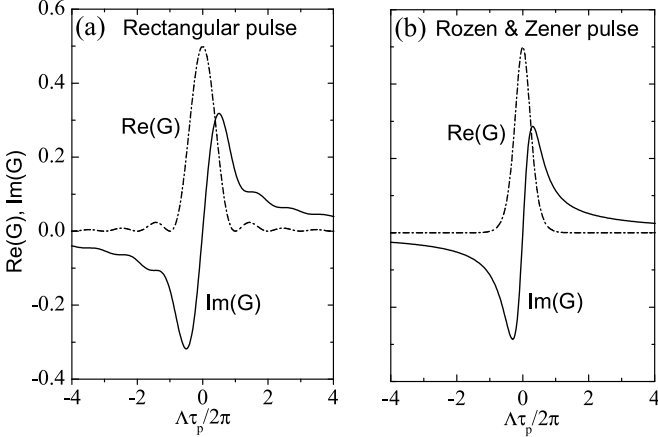


FIG. 6: The dependence of real and imaginary parts of G on detuning, $\Lambda = \omega_{\text{pr}} - \omega_0$. Dash-dot and solid curves are calculated, respectively, for (a) the rectangular and (b) Rosen&Zener pulses.

Figure 6 shows the real and imaginary parts of G calculated for the pulses of rectangular shape (panel (a)) and Rosen&Zener shape (panel (b)), respectively. For the both pulse shape the dependences $G(\Lambda)$ look qualitatively very similar. One can see that the Faraday and ellipticity signals are, respectively, odd and even functions of the detuning. Therefore, the ellipticity reaches its maximum sensitivity for zero detuning, $\Lambda = 0$, whereas the Faraday signal is most sensitive for the detuned probe pulses with $|\Lambda|\tau_p \approx 1$. The Kerr signal dependence on detuning has, in general, an asymmetric profile due to a combined contribution from \mathcal{F} and \mathcal{E} to its magnitude, see Eq. (59). As shown below, this different frequency sensitivity leads to the different time-resolved Faraday, Kerr and ellipticity signals in a QD ensemble with inhomogeneously broadened resonant transition energies.

C. Effective media approximation

At the end of this section we establish the link between the microscopic approach developed above and semi-phenomenological effective medium approximation which is a standard tool for the description of Faraday, Kerr and ellipticity effects in bulk systems. We demonstrate below that the effective medium approximation can describe the Faraday and Kerr effects in a 3D ensemble of QDs provided that the QD density satisfies certain conditions.

The irradiation of bulk homogeneous semiconductors with circularly polarized light creates non-equilibrium population of electrons and holes as well as non-equilibrium orientation of their spins and, thus, a nonequilibrium macroscopic magnetization. Hence, the semiconductor after the absorption of a circularly polarized pump pulse changes its dielectric and magnetic properties. These modifications can be tested by the linearly polarized probe light: the polarization plane rotates after its transmission through or reflection from the photoexcited medium leading to the Faraday and Kerr effects, respectively. The effects are phenomenologically described by the Fourier component of the displacement field, $\mathbf{D}(\omega)$, which is connected with the Fourier component of the electric field of the probe light, $\mathbf{E}(\omega)$, by

$$\mathbf{D} = \varepsilon_b \mathbf{E} + \delta \hat{\varepsilon} \mathbf{E} + i[\mathbf{E} \times \mathbf{g}]. \quad (63)$$

Here ε_b is the background dielectric constant, $\delta \hat{\varepsilon}$ is the spin-independent modification of the dielectric tensor $\hat{\varepsilon}$ due to the filling of the conduction- and valence-band edge states by the photoexcited carriers, and \mathbf{g} is the gyration vector pointing in the direction determined by the spin orientation \mathbf{S} of photoexcited carriers and the point-group symmetry of the system. In bulk cubic semiconductors $\mathbf{g} \propto \mathbf{S}$ and the tensor $\delta \hat{\varepsilon}$ reduces to a scalar $\delta \varepsilon$.

The same description can be used for the 3D ensemble of QDs if their concentration N_{QD}^{3D} satisfies two conditions. Firstly, N_{QD}^{3D} should be sufficiently small so that the QDs may be considered as independent dipoles. Secondly, N_{QD}^{3D} should be sufficiently large to have the typical distances between QDs smaller than the light wavelength. The satisfaction of these conditions allows one to neglect the non-locality of the QD response and represent the displacement field \mathbf{D} in the QD sample as

$$\mathbf{D}(\mathbf{r}, t) = \varepsilon_b \mathbf{E}(\mathbf{r}, t) + 4\pi \delta \mathbf{P}(\mathbf{r}, t), \quad (64)$$

where the optically induced dielectric polarization is related to the electric field by

$$\delta \mathbf{P}(\mathbf{r}, t) = \int_{-\infty}^t \hat{\chi}(t-t') \mathbf{E}(\mathbf{r}, t') dt'. \quad (65)$$

Using Eqs. (42), (43) we can present nonzero components of the tensor $\hat{\chi}(\tau)$ as

$$\chi_{xx}(\tau) = \chi_{yy}(\tau) = -N_{QD}^{3D} \frac{n_e - n_{tr}}{2i\hbar} |\mathcal{D}|^2 e^{-i\omega_0 \tau}, \quad (66)$$

$$\chi_{yx}(\tau) = -\chi_{xy}(\tau) = -N_{QD}^{3D} \frac{S_z - J_z}{\hbar} |\mathcal{D}|^2 e^{-i\omega_0 \tau}. \quad (67)$$

It follows then that the QD contribution to the frequency-dependent dielectric permittivity tensor can be written as⁴⁷

$$\begin{aligned} \varepsilon_{xx}(\omega) &= \varepsilon_{yy}(\omega) \\ &= \varepsilon_b + (n_e - n_{tr}) \frac{2\pi N_{QD}^{3D} |\mathcal{D}|^2}{\hbar(\omega_0 - \omega - i0)}, \\ \varepsilon_{yx}(\omega) &= -\varepsilon_{xy}(\omega) = (S_z - J_z) \frac{4\pi i N_{QD}^{3D} |\mathcal{D}|^2}{\hbar(\omega_0 - \omega - i0)}. \end{aligned} \quad (68)$$

Comparison with Eq. (63) shows that the gyration vector \mathbf{g} in the photoexcited QD medium has only one nonzero component,

$$g_z = (J_z - S_z) \frac{4\pi N_{QD}^{3D} |\mathcal{D}|^2}{\hbar(\omega_0 - \omega - i0)}, \quad (69)$$

which is proportional to the difference of spin densities of electrons and trions in the system and has a resonance at the trion excitation frequency. On the other hand, the modification of diagonal components of the dielectric tensor $\varepsilon_{xx} = \varepsilon_{yy}$ is proportional to the difference in population of the electron and trion levels irrespective to the their spin orientation.

IV. TIME-DEPENDENT TRACES OF PUMP-PROBE KERR AND FARADAY ROTATION AND ELLIPTICITY SIGNALS

In this section we apply the derived general expressions to calculate the typical time-dependent traces of two color pump-probe Faraday and Kerr rotation (FR

and KR) signals as well as the ellipticity created by short pulses of the resonant light and by a train of such pulses in an ensemble of singly charged QDs. The real QD structures possess two important properties that affect strongly the time dependent traces, but have not been considered in the previous sections. They are (i) inhomogeneity of a QD ensemble expressed in dispersion of the QD resonant transition energies and electron g -factors, and (ii) dispersion of electron precession frequencies connected with fluctuations of the nuclear contribution to these frequency. Here we conduct calculations for the QD ensemble assuming that the broadening of trion resonance frequency, dispersion of electron g -factors and fluctuations of the nuclear contributions to the electron spin precession frequency are similar to those in the samples studied in a series of works^{11,12,13,28}. Those samples contained 20 layers of InGaAs QDs self-organized during the molecular-beam epitaxy growth.

In the following calculations we neglect the scatter in the QD oscillator transition strengths and the nuclear induced frequency focusing effect²⁸. For illustrative purposes below we show the FR and ellipticity signals created by the electron spin polarization only. We neglect the trion J_z -dependent contribution to these signals in Eqs. (55) and (58) which affects the time dependence traces only during the trion recombination time $\tau_{QD} \approx 400$ ps¹³. As a result the calculated dependences can be directly compared with experimental data only for times longer than τ_{QD} .

A. Modeling of inhomogeneities in a QD ensemble

To model time dependences of the FR and ellipticity signals generated by the resonant pump pulses of circularly polarized light we assume that the distribution of the resonant transition energies, $\rho_{\text{opt}}(\omega_0)$, in the QD ensemble has the Gaussian form:

$$\rho_{\text{opt}}(\omega_0) = \exp\left[-\frac{\hbar^2(\omega_0 - \bar{\omega}_0)^2}{2(\Delta E)^2}\right], \quad (70)$$

where $\bar{\omega}_0$ is the average trion transition frequency and ΔE is the half-width of this distribution. The distribution is shown in Fig. 7. In the calculations we used $\hbar\bar{\omega}_0 = 1.4$ eV and $\Delta E = 6.5$ meV from Ref.¹¹. Only a small part of this distribution is excited by the pump pulse with $\tau_p = 1.5$ ps. This part is proportional to the pulse spectral width $\sim \hbar/\tau_p = 1.75$ meV and is centered at the pump carrier frequency ω_p . The photoexcited part of the QD distribution is shown in Fig. 7 by filled Gaussian at low-energy part of $\rho_{\text{opt}}(\omega_0)$.

The dispersion of the electron spin precession frequency in a QD ensemble is determined by the dispersion of electron g -factors and fluctuations of the nuclear contribution to the precession. The electron g -factor, g_e , depends generally on the effective energy gap of the QD, i.e. on the optical transition frequency, as well as on the QD shape and composition³⁸. The first effect gives rise to

a correlation between the average value of g -factor and the trion resonance frequency and can be approximated by a linear function

$$g_e(\omega_0) = A\hbar\omega_0 + C, \quad (71)$$

where A and C are fitting parameters. This results in the dependence of Larmor precession frequency, $\Omega_L(\omega_0) = \mu_B g_e(\omega_0) \mathbf{B} / \hbar$, on a trion optical resonance frequency, which is shown in Fig. 7 by thick inclined line. The spread of Ω_L connected with the g -factor dependence on an excitation frequency is controlled by the pump pulse width \hbar/τ_p . This spread is marked by a green/gray segment on a linear dependence of $\Omega_L(\omega_0)$ in Fig. 7. The distribution of electron spin precession frequencies, $\rho(\Omega_L)$ created by this effect is shown in the inset of Fig. 7 by filled Gaussian. We use in our calculations $A = -1.75 \mu\text{eV}^{-1}$ and $C = 2.99$ taken from the fit of experimental data in Ref.¹³.

The frequency dependent regular part of electron g -factor in Eq.(71) does not provide by itself a complete description of electron spin precession frequency dispersion connected with g -factor distribution. This dispersion in a QD ensemble is strongly affected by the QD shape and composition. The corresponding distribution of g -factors can be phenomenologically described by the Gaussian, $\rho_g(g_e)$, with the root mean square of electron g -factor distribution, Δg_e .

The dispersion of electron spin precession frequencies is affected also by fluctuations of hyperfine fields of nuclei that are collectively acting on the localized electron in a QD. The electron spin precession frequency $\Omega = \Omega_L + \omega_N = \mu_B g_e \mathbf{B} / \hbar + \omega_N$ contains a nuclear contribution, ω_N , which is proportional to the projection of the nuclear spin polarization on the external field (if external field is much larger than nuclear field fluctuations, which usually is the case)²⁸. The nuclear contribution is connected with statistical fluctuations of the nuclear spin polarization in a QD. The fluctuations are described by a Gaussian with the dispersion $\Delta\omega_N$ proportional to $N^{-1/2}$, where N is the number of nuclei in the QD volume⁴⁸. We ignore the nuclear induced frequency focusing effect⁴⁹, which could modify the density of electron spin precession mode to a comb-like shape in a QD ensemble exposed to a pulse train excitation Ref.²⁸.

The resulting broadening of electron spin precession frequencies connected with g -factor dispersion and with nuclear fluctuations, $\rho(\Omega) = \rho(\mu_B g_e B / \hbar + \omega_N)$ is also described by the Gaussian:

$$\rho(\Omega) = \frac{1}{\sqrt{2\pi}\Delta\Omega} \exp\left[-\frac{(\Omega - \Omega_L)^2}{2(\Delta\Omega)^2}\right], \quad (72)$$

where $\Omega_L(\omega_0) = \mu_B g_e(\omega_0) B / \hbar$ and $\Delta\Omega = \sqrt{(\mu_B \Delta g_e B / \hbar)^2 + (\Delta\omega_N)^2}$ is the total frequency dispersion. The range of electron spin precession frequencies generated by the pulse due to this dispersion is shown in Fig. 7 by crosshatched region around the linear dependence $\Omega_L(\omega_0)$. The calculations were conducted

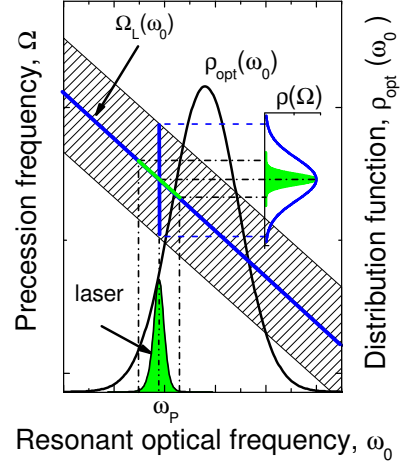


FIG. 7: Schematic illustration of the resonant transition energies distribution $\rho_{\text{opt}}(\omega_0)$ (black solid line) and the part of this distribution excited by short resonant pulse (green/gray profile). The range of Larmor frequencies created by the short pulse is shown by the crosshatched region around the linear dependence $\Omega_L(\omega_0)$. Inset shows the distribution of the electron spin precession frequencies $\rho(\Omega)$ with (blue/solid line) and without (filled green/gray area) shape and composition contribution to the g -factor dispersion and nuclear fluctuations.

for $\Delta g_e = 0.0037$ ¹³ and $\Delta\omega_N = 0.37$ GHz extracted from the amplitude of random nuclear fluctuation field of 7.5 mT⁵⁰. We assume that Δg_e and $\Delta\omega_N$ is independent of the QD resonance energy. One can see that for used set of Δg_e and $\Delta\omega_N$ the dispersion of electron spin precession frequencies $\rho(\Omega)$ is much broader than one created by the g -factor dependence on the excitation frequency (see inset in Fig. 7). This additional broadening leads to the fast dephasing of electron spin polarization and should be taken into account in a description of the time dependence of FR and ellipticity signals.

To obtain the time-dependent traces of the FR and ellipticity signals for the QD ensemble we average Eqs. (55) and (58) over the distribution of optical transition energies, $\rho_{\text{opt}}(\omega_0)$, described by Eq. (70) and over distribution of electron spin precession frequencies, $\rho(\Omega)$, described by Eq. (72). Without any calculations, however, one can notice from Eq. (55) that in degenerate case when $\omega_{\text{pr}} = \omega_p$, FR signal vanishes if S_z and J_z and all dispersion functions are even functions of the detuning, $\omega_{\text{pr}} - \omega_0$, because the signal is proportional to the odd function of detuning $\text{Im}[G(\omega_{\text{pr}} - \omega_0)]$. For degenerate case FR signal could arise for excitation at one side of $\rho_{\text{opt}}(\omega_0)$ distribution, or as a result of dependence of electron g -factors or oscillator transition strengths on the optical transition energy.

B. Effects of a single pump pulse

We start by considering the two color FR and ellipticity signals excited by a single pump pulse as function of the time delay between pump and probe pulses with frequencies ω_p and ω_{pr} , respectively. To clarify qualitative differences between FR and ellipticity signals we assume here and in the subsection IV C that $\rho_{opt}(\omega_0)$ is independent of ω_0 or, equivalently, that the resonant excitation of QDs is performed at the maximum of $\rho_{opt}(\omega_0)$, which is so broad that $\Delta E \gg \hbar/\tau_p$. To obtain nonvanishing FR signal, however, we take into account the dependence of an electron g -factor on the resonance transition frequency, ω_0 , see Eq. (71).

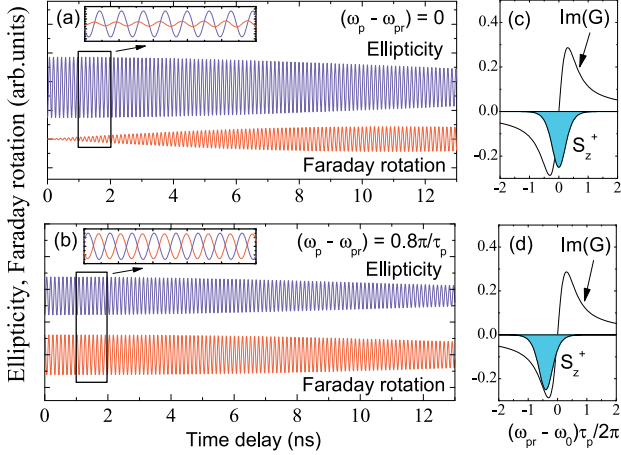


FIG. 8: Time resolved dependence of the pump-probe Faraday rotation and ellipticity signals initiated in the QD ensemble by a single pump pulse for (a) the degenerate, $\omega_p = \omega_{pr}$, and (b) nondegenerate, $\omega_p \neq \omega_{pr}$, regimes. For clarity, the signals are vertically shifted from each other. Calculations are conducted for the pump pulse with area $\Theta = \pi$ in the magnetic field $B = 1$ T by using g -factor spectral dependence described by Eq. (71) and the parameters $\tau_p = 1.5$ ps, $\hbar\omega_{pr} = 1.4$ eV and $\tau_{s,e} = 3$ μ s taken from Ref.¹¹. Insets show the Faraday rotation and ellipticity signals in a small range of delay times. Faraday rotation curve in inset in panel (a) is multiplied by a factor of 2. Panels (c) and (d) show S_z^+ and $\text{Im}[G(\omega_{pr} - \omega_0)]$ as a function of $\omega_{pr} - \omega_0$ for the degenerate and nondegenerate regimes, respectively.

Figure 8(a) shows the traces of FR and ellipticity signals for degenerate case ($\omega_p = \omega_{pr}$) calculated in a magnetic field $B = 1$ T for the QD ensemble with the average g -factor, its dependence on ω_0 and $\tau_{s,e}$ extracted from the data of Refs.^{11,13}. The trace of the ellipticity signal demonstrates damped oscillations with the decay determined by the dispersion of electron spin precession frequencies.

Figure 8(a) shows also that the FR signal is absent at zero delay time, as it was expected, due to symmetric distribution S_z and $\rho_{opt}(\omega_0)$ around pumping frequency. Surprisingly, however, this signal is growing in time. This

happens because the electron spin distribution created by the pump pulse being initially symmetric around ω_p (see Fig. 8(c)) is gradually losing its symmetry due to different Larmor precession frequencies on the low- and high-energy wings of the QD distribution as described by Eq. (71). This imbalance of the electron spin polarization connected with electron g -factor dependence on ω_0 results in the growth of the FR signal with time. The inset in Fig. 8(a) shows also a phase shift between the Faraday rotation and ellipticity signals. Calculations show (not presented) that oscillation frequencies of the FR and ellipticity signals are also slightly different. The effect is connected with different spectral contributions to the FR and ellipticity and results in a weak time dependence of the phase shift.

Figure 8(b) shows FR and ellipticity signals for the nondegenerate case where pump and probe pulses are detuned: $\omega_p - \omega_{pr} = 0.8\pi/\tau_p$. The electron spin polarization created in this case is not a symmetric function of $\omega_{pr} - \omega_0$ as one can see in Fig. 8(d), and the probe light measures the electron spin polarization only at one of the spin distribution wings. Therefore, at $t = 0$ the FR signal is nonzero and its time dynamics is qualitatively similar to that of the ellipticity signal. It is seen from inset in Fig. 8(b) that the phase shift between Faraday rotation and ellipticity signals is close to π . The phase shift and the sign of the FR signal, correspondingly, depends on the sign of the pump-probe detuning because $\text{Im}[G(\omega_{pr} - \omega_0)]$ is an odd function of the detuning.

C. Effects of an infinite train of pump pulses

Figure 9 shows the time dependent traces of the FR and ellipticity signals initiated by a train of short pulses of circularly polarized light with the repetition period $T_R = 13.2$ ns in degenerate regime $\omega_p = \omega_{pr}$. Calculations were conducted for the pulse duration $\tau_p = 1.5$ ps and magnetic fields $B = 1$ T and $B = 5$ T (panels (a) and (b), correspondingly). Panel (c) shows the results calculated for $\tau_p = 100$ fs and $B = 1$ T. The commonly used repetition period of the mode-locked lasers T_R is about 10 ns, which is much shorter than the typical electron spin relaxation time in a QD. As a result the infinite train of such pulses creates a stationary distribution of rotating spin polarization $S_z(\Omega; t)$, which modifies strongly the FR and ellipticity signals from those created by a single pump pulse. The traces in Figs. 9(a), (b) and (c) are calculated by using the steady-state values of the electron spin polarization defined by Eq. (29). Here, like in the previous subsection, the dispersion of electron spin precession frequency is described by the function $g_e(\omega_0)$ given by Eq. (71). Figures 9(d), (e) and (f) show the electron spin distributions at the moment right after the pump pulse arrival. One can see that the latter distributions are very different from those created by a single pulse and shown in Figs. 8(c) and 8(d).

In the case of excitation of QD ensemble by an infinite

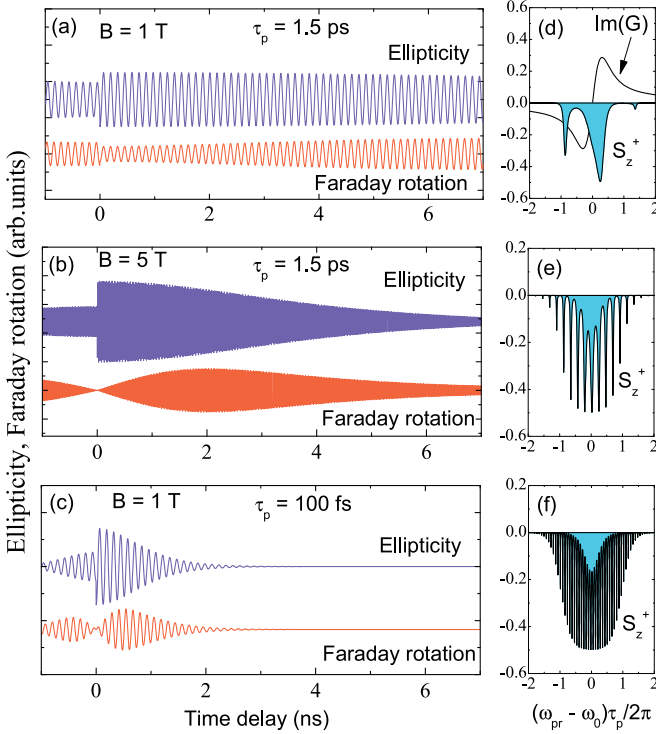


FIG. 9: Time resolved dependence of the single color pump-probe Faraday rotation and ellipticity signals initiated in the QD ensemble by a train of pump pulses with the repetition period $T_R = 13.2$ ns and pulse duration $\tau_p = 1.5$ ps ((a) and (b)) and $\tau_p = 100$ fs (c), in the magnetic fields $B = 1$ T (a) and (c), and $B = 5$ T (b). Calculations are conducted for pump pulses with the area $\Theta = \pi$ using g -factor spectral dependence described by Eq. (71) and the parameters $\hbar\omega_{pr} = 1.4$ eV and $\tau_{s,e} = 3$ μ s taken from Ref.¹¹. Panels (d), (e) and (f) show the distributions $S_z^+(\omega_{pr} - \omega_0)$ and $\text{Im}[G(\omega_{pr} - \omega_0)]$ created by the pico- and femtosecond pulse trains at $B = 1$ T and $B = 5$ T, respectively.

pump pulse train a steady state distribution of electron spin polarization is formed in accordance with Eq. (29). The modes satisfying the PSC: $\Omega = 2\pi N/T_R$ (N is a large integer, $N \approx 100$ for $B = 1$ T) provide an enhanced contribution to the electron spin polarization. The sum of these mode contributions to the spin polarization results in the constructive interference around the pulse arrival time due to the commensurability of the spin precession frequencies with the cyclic repetition frequency of the train, $2\pi/T_R$.

The shape of the steady state distribution of electron spin polarization depends strongly on the number of precession modes, which satisfy PSC and, therefore, on pulse duration and on a magnetic field. At the relatively weak field, $B = 1$ T, and pulse duration $\tau_p = 1.5$ ps the distribution is asymmetric because only few modes satisfy PSC (see Fig. 9(d)). In this case, the ellipticity and Faraday rotation signals are similar to each other analogously to the situation of detuned pump and probe, Fig. 8(b).

There are more modes satisfying PSC with increase

of a magnetic field. This is because the dispersion of electron spin precession frequency increases linearly with magnetic field but the distance between the PSC modes $2\pi/T_R$ does not change. The density of the mode satisfying the PSC increases and the steady state distribution of electron spin precession frequency at the moment of pulse arrival becomes more dense and symmetric (see Fig. 9(e), where the electron spin polarization was calculated for $B = 5$ T). In this case the Faraday rotation signal and the ellipticity signal become phase shifted relative to each other. More importantly, the Faraday signal vanishes at zero delay between pump and probe pulses (Fig. 9(b)) similar to that for the case the single pulse excitation with degenerate pump and probe pulses (c.f., Fig. 8(a)). The shortening of the pulse duration ($\tau_p = 100$ fs) also leads to an increase of the number of modes satisfying PSC as it is clearly seen in Fig. 8(f), because of the spectral width of the laser pulse increases with shortening of the pulse duration. The increase number of modes results in faster decay of ellipticity and FR rotation signals and in vanishing of the Faraday rotation signal at the moment of pulse arrival. In two-color experiments (not shown) the ellipticity and the Faraday rotation signal time dependent traces become similar and the phase shift vanishes.

D. Effect of the pump and probe spectral position and the electron g -factor dispersion

Now we turn to the effects of the spectral distribution of the QD transition energies and of the distribution of electron spin precession frequencies described by Eqs. (70) and (72) on the time traces of the FR and ellipticity signals created by the train of pulses with repetition period $T_R = 13.2$ ns. Panels (a)-(c) in Fig. 10 show FR and ellipticity time-resolved dependences for different spectral positions of pump and probe pulses which are shown on the corresponding right-hand side panels. The panels (a) and (b) show the traces for the same pump and probe carrying frequencies (single color or degenerate pump-probe setup). This frequencies are tuned to the peak of QD distribution in Fig. 10(a) and to its left wing in Fig. 10(b). The panel (c) shows the traces of the FR and ellipticity signals for the case when the pump and probe pulse frequencies are in the vicinity of the maximum of $\rho_{opt}(\omega_0)$ but they are slightly detuned with respect to each other. The distribution of optical transition frequencies in the QD ensemble, $\rho_{opt}(\omega_0)$, shown in Fig. 10 by black curves is described by Eq. (70). The calculation shows that the inclusion of additional dispersion of electron spin precession frequencies described by Eq. (72) leads to the faster decay of both the FR and ellipticity signals due to a faster dephasing of electron spin precession in the QD ensemble. It is worth noting that the FR signal amplitude vanishes for degenerate pump and probe pulses tuned to the maximum of the QD distribution, similarly to what was experimentally observed

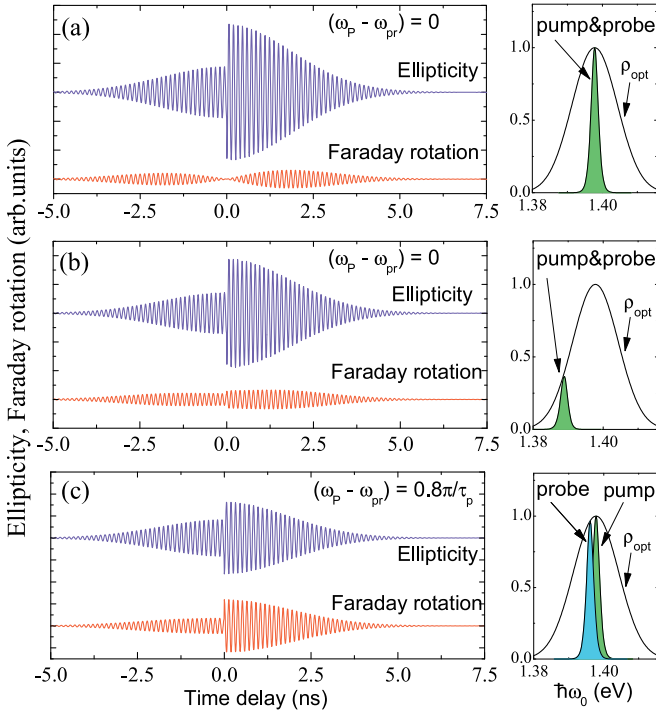


FIG. 10: Time resolved dependence of the pump-probe Faraday rotation and ellipticity signals initiated in the QD ensemble by a train of pump pulses for the degenerate, $\omega_p = \omega_{pr}$, (panels (a) and (b)) and nondegenerate, $\omega_p \neq \omega_{pr}$, (panel (c)) regimes. In the right-hand side panels we show the density of the optical transition energies and the frequency position of the pump and probe pulses. Calculations are conducted for pump pulses of the area $\Theta = \pi$, the magnetic field $B = 1$ T, $\tau_p = 1.5$ ps, and $\tau_{s,e} = 3$ μ s.

in Ref.⁵¹. The nonzero FR signal at zero delay time seen in Figs. 10(b) and 10(c) is related to the asymmetry in the QD density distribution which is revealed in the case of pump pulse detuned from the $\bar{\omega}_0$ ($\hbar\bar{\omega}_0 = 1.4$ eV). In the case of two color experiments, traces of the pump-probe FR and ellipticity signals are very similar as it is seen in Fig. 10(c).

Figure 11 compares the Faraday rotation and ellipticity signals for laser trains with different pulse duration: 1.5 ps (a) and 100 fs (b). Calculations that take into account spectral distribution of optical transition energies in the QD ensemble $\rho_{opt}(\omega_0)$ and total Larmor frequency dispersion where conducted in degenerate regime for resonant excitation of QDs at the maximum of $\rho_{opt}(\omega_0)$ ($\omega_p = \omega_{pr} = \omega_0$). The case of ps-excitation differs from one demonstrated in Fig. 10(a) only by larger dispersion of electron spin precession modes $\Delta\Omega = 0.9$ GHz (time dependent traces in Fig. 10(a) were calculated for $\Delta\Omega = 0.5$ GHz) and, therefore, they show faster decay of the signals. The spectral width of pulses in the fs-pulse train is larger than the distribution $\rho_{opt}(\omega_0)$ used in this calculation. This effectively decreases the number of electron spin precession modes contributing to the FR and ellipticity signals explaining dephasing decay, which

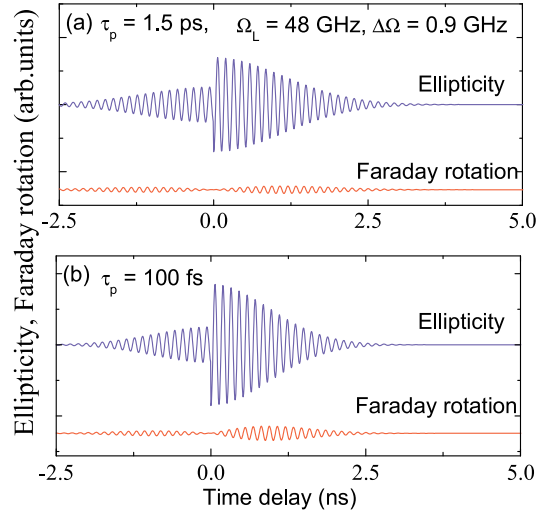


FIG. 11: Time resolved dependences of the degenerated pump-probe Faraday rotation and ellipticity signals in inhomogeneous ensemble of QDs excited by trains of pulses with duration 1.5 ps (panel (a)) and 100 fs (panel (b)), correspondingly. Calculations are conducted for the set of parameters the same as in Figs. 9(a) and 9(c). Note, that the time scale used here is different from the time scale used in Fig. 9.

is slightly weaker than the decay shown in Figure 9(c).

Surprisingly, Fig. 11 shows that signals created by ps- and fs-pulse trains are very similar and the signal decays are almost the same. This could occur only if numbers of electron precession modes satisfying the PSC for both excitations are comparable. In the case of ps-train excitation the dispersion of electron spin precession modes is controlled by Δg and $\Delta\omega_N$ connected with the shape and composition fluctuations of QDs and the nuclear field fluctuations, correspondingly. Due to the small spectral width of the ps-excitation only a small part of the electron spin precession mode dispersion is determined by the frequency dependence of the electron g -factor. This is not the case, however, for fs-pulse train excitation, where the dispersion of electron spin precession modes have significant contribution connected with frequency dependence of an average g -factor $g(\omega_0)$ on the spectral width of the fs-pulses.

Finally, Fig. 12 shows traces of the KR signal calculated by using Eq. (59) for three different thicknesses of the cap layer and the same parameters as in Fig. 10. One can see that, for particular cap layer thicknesses, the KR signal looks like the either FR or ellipticity signals. However, in general the trace of the KR signal is a linear combination the FR and ellipticity signals with their partial contributions depending on the cap layer thickness.

Note that $L = \lambda/2n_b$ (top curves in Fig. 12) corresponds to the real thickness $L = 115$ nm of cap layer of the QD sample which was investigated in Ref.¹¹. For this cap layer time dependent trace of the KR signal is similar to that of the ellipticity signal.

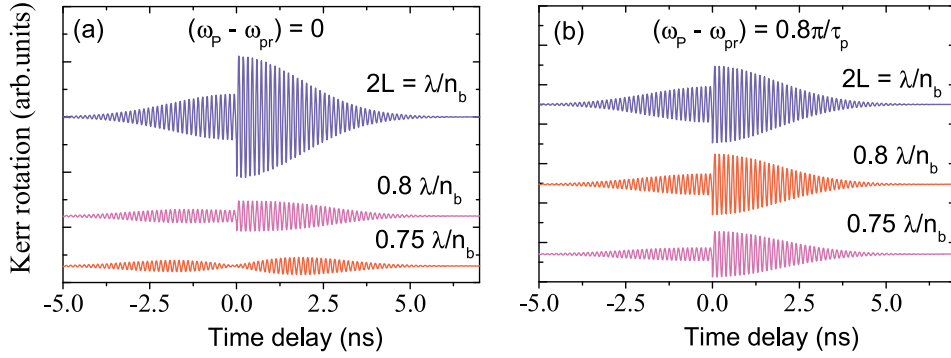


FIG. 12: Time resolved dependence of pump-probe Kerr rotation signals initiated in the QD ensemble by a train of pump pulses for the degenerate (panel (a)) and nondegenerate (panel (b)) regimes. The traces are calculated for three thicknesses of the cap layer $2L = \lambda/n_b$, $0.8\lambda/n_b$, and $0.75\lambda/n_b$, where $n_b \equiv \sqrt{\epsilon_b}$. Calculations are conducted for the set of parameters the same as in Figs. 10(a) and 10(c).

V. SUMMARY

The formalism presented here provides a complete theoretical description of single- and two-color pump-probe Faraday or Kerr rotation and ellipticity experiments in an ensemble of singly charged QDs. The analytical expressions describing the electron spin polarization created by a circularly polarized pump pulse or by a train of such pulses are derived. The expressions for the magnitudes of the Faraday, Kerr and ellipticity signals are presented.

The developed theory shows that the pump-probe Faraday rotation and ellipticity experiments measure the electron spin precession in slightly different subsets of QDs of the ensemble leading to the different oscillation frequencies and shapes of the corresponding time-dependent traces. The time-dependent traces of the pump-probe Kerr rotation signal are linear superpositions of the Faraday rotation and ellipticity signals whose relative weights depend on the cap layer thickness.

The modeling of time-dependent traces of the Faraday rotation signal shows their high sensitivity to the inhomogeneous properties of the QD ensemble, such as

the transition-frequency dependence of electron g -factor and the nuclear-induced dispersion, as well as to the excitation conditions, such as pump and probe pulse detuning, single pulse versus train of pulses excitation, and the pumping intensity. The pump-probe Faraday and Kerr rotation and ellipticity experiments can provide a complementary information about inhomogeneous properties of QD ensembles.

ACKNOWLEDGMENTS

The authors thank M. Bayer and D. R. Yakovlev for the encouraging discussions and support as well as hospitality at the TU Dortmund University, I. V. Ignatiev and S. Carter for useful comments on the manuscript. I. A. Y., M. M. G. and E. L. I. acknowledge the financial support from RFBR, Programmes of RAS and the Deutsche Forschungsgemeinschaft (SPP1285). A. L. E. acknowledges support of the Office of Naval Research and Alexander-von-Humboldt Foundation. M. M. G. is grateful to the “Dynasty” Foundation — ICFPM.

¹ S. A. Wolf, D. D. Awschalom, R. A. Buhrman, J. M. Daughton, S. von Molnar, M. L. Roukes, A. Y. Chtchelkanova, and D. M. Treger, *Science* **294**, 1488 (2001).

² *Semiconductor Spintronics and Quantum Computation*, Eds. D. D. Awschalom, D. Loss, and N. Samarth (Springer-Verlag, Berlin, 2002).

³ J. M. Kikkawa and D. D. Awschalom, *Phys. Rev. Lett.* **80**, 4313 (1998).

⁴ J. M. Kikkawa, I. P. Smorchkova, N. Samarth, and D. D. Awschalom, *Science* **277**, 1284 (1997).

⁵ B. Beschoten, E. Johnston-Halperin, D. K. Young, M. Poggio M, J. E. Grimald, S. Keller, S. P. DenBaars, U. K. Mishra, E. L. Hu, and D. D. Awschalom, *Phys Rev B* **63**, 121202 (2001).

⁶ T. A. Kennedy, A. Shabaev, M. Scheibner, Al. L. Efros,

A. S. Bracker, and D. Gammon, *Phys. Rev. B* **73**, 045307 (2006).

⁷ E. A. Zhukov, D. R. Yakovlev, M. Bayer, M. M. Glazov, E. L. Ivchenko, G. Karczewski, T. Wojtowicz, and J. Kossut, *Phys. Rev. B* **76**, 205310 (2007).

⁸ W. J. H. Leyland, G. H. John, R. T. Harley, M. M. Glazov, E. L. Ivchenko, D. A. Ritchie, I. Farrer, A. J. Shields, and M. Henini, *Phys. Rev. B* **75**, 165309 (2007).

⁹ J. A. Gupta, D. D. Awschalom, X. Peng, and A. P. Alivisatos, *Phys. Rev. B* **59** R10421 (1999); J. A. Gupta, D. D. Awschalom, Al. L. Efros, and A. V. Rodina, *Phys. Rev. B* **66**, 125307 (2002).

¹⁰ R. Epstein, D. T. Fuchs, W. V. Schoenfeld, P. M. Petroff, and D. D. Awschalom, *Appl. Phys. Lett.* **76**, 733 (2001).

¹¹ A. Greilich D. R. Yakovlev, A. Shabaev, Al. L. Efros, I. A.

- Yugova, R. Oulton, I. V. Stavarache, D. Reuter, A. Wieck, and M. Bayer, *Science* **313**, 341 (2006).
- ¹² A. Greilich, M. Wiemann, F. G. G. Hernandez, D. R. Yakovlev, I. A. Yugova, M. Bayer, A. Shabaev, Al. L. Efros, D. Reuter, and A. D. Wieck, *Phys. Rev. B* **75**, 233301 (2007).
- ¹³ A. Greilich, R. Oulton, E. A. Zhukov, I. A. Yugova, D. R. Yakovlev, M. Bayer, A. Shabaev, Al. L. Efros, I. A. Merkulov, V. Stavarache, D. Reuter, and A. Wieck, *Phys. Rev. Lett* **96**, 227401 (2006).
- ¹⁴ J. Kikkawa and D. D. Awschalom, *Nature* **397**, 139 (1999).
- ¹⁵ S. A. Crooker and D. L. Smith, *Phys. Rev. Lett.* **94**, 236601 (2005).
- ¹⁶ J. Stephens, J. Berezovsky, J. P. McGuire, L. J. Sham, A. C. Gossard, and D. D. Awschalom, *Phys. Rev. Lett.* **93**, 097602 (2004).
- ¹⁷ S. A. Crooker, M. Furis, X. Lou, C. Adelmann, D. L. Smith, C. J. Palmstrom, and P. A. Crowell, *Science* **309**, 2191 (2005); M. Furis, M. D. L. Smith, S. Kos, E. S. Garlid, K. S. M. Reddy, C. J. Palmstrom, P. A. Crowell, and S. A. Crooker, *New J. Physics* **9**, 347 (2007).
- ¹⁸ Y. K. Kato, R. C. Myers, A. C. Gossard, and D. D. Awschalom, *Science* **306**, 1910 (2004).
- ¹⁹ V. Sih, W. H. Lau, R. C. Myers, V. R. Horowitz, A. C. Gossard, and D. D. Awschalom, *Phys. Rev. Lett.* **97**, 096605 (2006).
- ²⁰ *Optical Orientation*, Eds. F. Meier and B.P. Zakharchenya (North-Holland, Amsterdam, 1984).
- ²¹ D. D. Awschalom, J. M. Halbout, S. von Molnar, T. Siegrist, and F. Holtzberg, *Phys. Rev. Lett.* **55**, 1128 (1985).
- ²² J. J. Baumberg, D. D. Awschalom, N. Samarth, H. Luo, and J. K. Furdyna, *Phys. Rev. Lett.* **72**, 717 (1994).
- ²³ J. J. Baumberg, S. A. Crooker, D. D. Awschalom, N. Samarth, H. Luo, and J. K. Furdyna, *Phys. Rev. B* **15**, 7689 (1994).
- ²⁴ N. I. Zheludev, M. A. Brummell, A. Malinowski, S. V. Popov, R. T. Harley, D. E. Ashenford, and B. Lunn, *Solid State Commun.* **89**, 823 (1994).
- ²⁵ J. R. Petta, A. C. Johnson, J. M. Taylor, E. A. Laird, A. Yacoby, M. D. Lukin, C. M. Marcus, M. P. Hanson, and A. C. Gossard, *Science* **309**, 2180 (2005).
- ²⁶ R. I. Dzhiyev, B. P. Zakharchenya, V. L. Korenev, and M. N. Stepanova, *Fiz. Tverd. Tela* **39**, 1975 (1997) [*Phys. Solid State* **39**, 1765 (1997)].
- ²⁷ A. Shabaev, A. L. Efros, D. Gammon, and I. A. Merkulov, *Phys. Rev. B* **68**, 201305(R) (2003).
- ²⁸ A. Greilich, A. Shabaev, D. R. Yakovlev, Al. L. Efros, I. A. Yugova, D. Reuter, A. D. Wieck, and M. Bayer, *Science* **317**, 1896 (2007).
- ²⁹ A. Greilich, S. Spatzek, I. A. Yugova, I. A. Akimov, D. R. Yakovlev, Al. L. Efros, D. Reuter, A. D. Wieck, and M. Bayer, *Phys. Rev. B* **79**, 201305(R) (2009).
- ³⁰ A. Greilich, S. E. Economou, S. Spatzek, D. R. Yakovlev, D. Reuter, A. D. Wieck, T. L. Reinecke, and M. Bayer, *Nature Physics* **5**, 262 (2009).
- ³¹ S. E. Economou and T. L. Reinecke, *Phys. Rev. Lett.* **99**, 217401 (2007).
- ³² A. G. Aronov and E. L. Ivchenko, *Fiz. Tverd. Tela* **15**, 231 (1973) [*Sov. Phys. Solid State* **15**, 160 (1973)].
- ³³ Th. Östreich, K. Schnhammer, and L. J. Sham, *Phys. Rev. Lett.* **74**, 4698 (1995).
- ³⁴ N. Linder and L. J. Sham, *Physica E* **2**, 412 (1998).
- ³⁵ S. A. Crooker, D. D. Awschalom, J. J. Baumberg, F. Flack, N. Samarth, *Phys. Rev. B* **56**, 7574 (1997).
- ³⁶ A. K. Zvezdin and V. A. Kotov, *Modern Magnetooptics and Magneto-optical Materials* (Institute of Physics Publishing, Bristol, 1997).
- ³⁷ For example see: M. V. Gurudev Dutt, J. Cheng, Y. Wu, X. Xu, D. G. Steel, A. S. Bracker, D. Gammon, S. E. Economou, R.-B. Liu, and L. J. Sham, *Phys. Rev. B* **74**, 125306 (2006).
- ³⁸ E. L. Ivchenko, *Optical Spectroscopy of Semiconductor Nanostructures* (Alpha Science, Harrow UK, 2005).
- ³⁹ A. Esser, E. Runge, R. Zimmermann, and W. Langbein, *Phys. Rev. B* **62**, 8232 (2000).
- ⁴⁰ M. A. Semina, R. A. Sergeev, and R. A. Suris, *Physica E* **40**, 1357 (2008).
- ⁴¹ V. I. Arnold, *Geometrical Methods in the Theory of Ordinary Differential Equations*, in Springer Series of Comprehensive Studies of Mathematics, Springer-Verlag 2nd ed. (1996).
- ⁴² N. Rosen and C. Zener, *Phys. Rev.* **40**, 502 (1932).
- ⁴³ M. M. Glazov and E. L. Ivchenko, *Semiconductors* **42**, 951 (2008).
- ⁴⁴ G. V. Astakhov, M. M. Glazov, D. R. Yakovlev, E. A. Zhukov, W. Ossau, L. W. Molenkamp, and M. Bayer, *Semicond. Sci. Technol.* **23**, 114001 (2008).
- ⁴⁵ Here we consider only one term, which is proportional to $e^{-i\omega_{pr}t}$, for the complex conjugate term the calculation is analogous.
- ⁴⁶ E. A. Zhukov, D. R. Yakovlev, M. Bayer, G. Karczewski, T. Wojtowicz, and J. Kossut, *Phys. Status Solidi B* **243**, 878 (2006); G. V. Astakhov, T. Kiessling, D. R. Yakovlev, E. A. Zhukov, M. Bayer, W. Ossau, B. P. Zakharchenya, G. Karczewski, T. Wojtowicz, and J. Kossut, *Phys. Status Solidi B* **243**, 858 (2006).
- ⁴⁷ L. D. Landau and E. M. Lifshitz, *Electrodynamics of Continuous Media (vol. 8)* (Butterworth-Heinemann, Oxford, 2004).
- ⁴⁸ I. A. Merkulov, Al. L. Efros, and M. Rosen, *Phys. Rev. B* **65**, 205309 (2002).
- ⁴⁹ These modifications have no general nature: they depend on many different parameters, particularly, on details of sample optical excitation and should be considered separately for each QD ensemble. In addition the modification of the electron spin precession frequency by the nuclei requires some time and should not affect the FR, KR and ellipticity signals during long times of nuclear spin dynamics. The light induced nuclear polarization also can be eliminated by the microwave field.
- ⁵⁰ M. Yu. Petrov, I. V. Ignatiev, S. V. Poltavtsev, A. Greilich, A. Bauschulte, D. R. Yakovlev, and M. Bayer, *Phys. Rev. B* **78**, 045315 (2008).
- ⁵¹ A. Greilich, S. Spatzek, Al. L. Efros, I. A. Yugova, D. R. Yakovlev, D. Reuter, A. D. Wieck, and M. Bayer, *Phys. Status Solidi C* **6**, 428 (2009).